Journal of Drug Delivery Science and Technology 121 (2026) 108326

Contents lists available at ScienceDirect

Journal of Drug Delivery Science and Technology

journal homepage: www.elsevier.com/locate/jddst

Improving the efficacy of platinum-chemotherapy with the smart polymer poly(sodium acrylate)

E.G. Whitty [a], I. Sousa [a,b], M. Gaborieau [b,c], P. Castignolles [b,d], R. Callaghan [a,e,*]

[a] Research School of Biology, and the Medical School, Australian National University, Canberra, ACT, 2601, Australia
[b] Australian Centre for Research on Separation Science (ACROSS), Western Sydney University, School of Science and Health, Locked Bag 1797, Penrith, New South Wales, 2751, Australia
[c] Karlsruhe Institute of Technology (KIT), Institute of Chemical Technology and Polymer Chemistry, Engesserstrasse 18, Karlsruhe, 76131, Germany
[d] Sorbonne Université, Institut Parisien de Chimie Moléculaire, Equipe Chimie des Polymères, 4 place Jussieu, Paris, 75005, France
[e] School of Health, Medicine and Life Sciences, University of Hertfordshire, Hatfield, Hertfordshire, AL10 9AB, United Kingdom

ARTICLE INFO

Keywords:
Smart polymer
Cisplatin
Cancer chemotherapy
Drug delivery system
Drug resistance
Branched polymer
Polymer uptake
poly(sodium acrylate)

ABSTRACT

Cisplatin and its derivatives are widely used in cancer chemotherapy; however, their clinical efficacy is hampered by instability, inherent reactivity and a poor pharmacokinetic profile. The "smart" polymer poly(sodium acrylate) (PNaA) may overcome these issues by ensuring the delivery of high cisplatin concentrations to the tumour site. PNaA is predicted to release drug cargo in a pH-dependent manner and is available in multiple branching topologies. Native (drug free) PNaA exhibited minimal impact on cell cycle progression and induced negligible levels of apoptosis, highlighting its inherent safety profile. In contrast, cisplatin delivered by PNaA, in all three branching topologies, displayed markedly improved cytotoxicity to colon adenocarcinoma and ovarian cancer cell lines. Surprisingly, there was no pH-dependency in the cytotoxic potency of the cisplatin-PNaA complex, which implies an alternative mechanism of action. Analysis by capillary electrophoresis demonstrated that cisplatin release from PNaA occurred over an extended 12-24 h period, whereas the cell cytotoxicity of loaded polymer occurred over 1 h. To further investigate the mechanism, a fluorescent derivative of PNaA was generated and it revealed a rapid cellular uptake and punctate localisation in the perinuclear region. Our data indicate that PNaA is an inert polymer capable of delivering cisplatin to cells using a mechanism that involves rapid intracellular accumulation of the drug-polymer complex. The mechanism was highly successful in improving the anticancer efficacy of cisplatin and can overcome a drug resistant phenotype, thereby rendering it a promising tool to improve chemotherapy.

1. Introduction

Chemotherapy provides an important treatment option for cancer in frontline, adjuvant and palliative settings. Combination chemotherapy regimens comprise conventional genotoxic or the more sophisticated molecularly targeted therapies. It is estimated that half of all chemotherapy regimens involve platinum containing anticancer drugs, with cisplatin, carboplatin and oxaliplatin the mainstays of treatment [1]. The most widely used clinical settings for cisplatin and its chemical derivatives are in the management of gastrointestinal, oesophageal, genitourinary and ovarian cancers. Cisplatin inhibits cell proliferation using a mechanism that involves extensive covalent modification of DNA, ultimately overwhelming repair processes to elicit apoptosis [2,3]. The efficacy of cisplatin is limited by several pharmacokinetic factors such as the presence of resistance mechanisms and a short serum half-life due to its inherent reactivity [4]. To overcome these problems, numerous synthetic chemistry strategies have developed platinum containing anticancer drugs with different leaving group chemical properties, using the Pt^{4+} oxidation state or employing distinct compound geometries [3]. Unfortunately, despite numerous and exhaustive medicinal chemistry efforts, the inherent pharmacokinetic issues remain, although a number of alternative strategies continue to be developed to improve the efficacy of platinum chemotherapy [5,6].

Although platinum anticancer drugs are plagued by pharmacokinetic inadequacies or resistance mechanisms, they retain clinical efficacy and thereby justify continued development of new compounds [7]. However, drug development occurs over a long time span due to the necessary regulatory processes and the overwhelming majority of lead

* Corresponding author. School of Health, Medicine and Life Sciences, University of Hertfordshire, Hatfield, Hertfordshire, AL10 9AB, United Kingdom.
E-mail address: R.Callaghan@herts.ac.uk (R. Callaghan).

https://doi.org/10.1016/j.jddst.2026.108326
Received 31 October 2025; Received in revised form 2 April 2026; Accepted 11 April 2026
Available online 16 April 2026

compounds fail to reach the market due to pharmacokinetic problems. Drug delivery systems are capable of circumventing pharmacokinetic issues by improving drug stability, increasing drug concentration at the tumour site and specific delivery to the tumour will reduce dose-limiting toxicity to normal tissues. Platinum containing anticancer compounds stand to gain significantly from the potential advantages of drug delivery systems.

The most widely used drug delivery systems are liposomes, which are composite structures comprising a lipid membrane bilayer and an aqueous central cavity [8]. The latter can accommodate high concentrations of cisplatin, a hydrophilic compound with aqueous solubility. Although several liposome formulations are FDA approved for clinical use [9], their efficacy is limited by avid clearance from the systemic circulation due to uptake in the macrophage phagocytic system located in reticular connective tissue such as the spleen and lymph nodes [10,11]. Like the liposomal formulations, the highly structured carbon nanotube delivery systems also contain an internal cavity that permits high cargo loading. However, these carbon-based structures display a propensity to aggregate due to their poor solubility in aqueous media and this property leads to a short circulatory system half-life [12,13].

An alternative to the cavity containing delivery systems described above are polymers that may be formed from biological or synthetic monomer units. Polymers typically require direct chemical links with the drug cargo and will display simple linear or complex 3-D structures with extensive branching. Synthetic polymers have the advantage of countless chemical properties that enable optimised cargo interaction, a mechanism for *in vivo* detection or the ability to attach tumour-targeting ligands. In addition, stimuli-responsive (smart) polymers provide cargo release under specific environmental triggers including pH, heat, light and electric or magnetic fields [14–17].

Polymers with pH-sensitive cargo release mechanisms are ideal candidates for drug delivery to the acidic extracellular environment of solid tumours. A promising candidate is poly(sodium acrylate), which we have shown has numerous advantageous properties [18]. Poly (acrylic acid) (PAA) undergoes a change in ionisation state to poly(sodium acrylate) (PNaA) under alkaline conditions, thereby rendering carboxylate groups available for loading of compounds containing charged or hydrophilic moieties [19,20]. It is this pH-responsiveness that classifies PNaA/PAA as a smart polymer as described [21–23]. Furthermore, the ability to generate poly(sodium acrylate) polymers with branching structures offer potential for higher loading capacity and delayed cargo release properties [19]. Our consortium has developed two branching structures for PNaA, including a 3-arm star topology consisting of a single core with three short-chain branched arms of similar length emerging. The second is a hyperbranched topology with densely packed short and long arms.

The physical and chemical properties of PNaA provide many optimal features of a drug delivery system and our objective is to assess the capability using an *in vitro* approach. Of relevance will be the loading capacity and whether the branched structures provide increased loading or sustained release kinetics. Using an *in vitro*, cellular approach will enable us to develop a mechanistic understanding of the polymer and whether it is capable of exploiting the acidic tumour microenvironment for cargo delivery. Ideally, PNaA will exhibit low or negligible inherent toxicity to cells and simply provide an inert and effective carrier. However, to justify further development and refinement, the use of PNaA should provide a significant increase in the efficacy of cisplatin to inhibit cancer cell proliferation.

2. Materials & methods

2.1. Poly(sodium acrylate) – materials and synthesis

Cisplatin was obtained from Merck (NSW, Australia). Linear PNaA (L-PNaA) was generated by living anionic polymerisation of *t*-butyl acrylate followed by a deprotection step. Branched PNaAs were obtained by controlled radical polymerisation (nitroxide-mediated polymerisation, see Figure A3) [19,24]. The 3-arm star PNaA (3-PNaA) has a single core with 3 arms of similar length bearing short branches and the hyperbranched PNaA (H-PNaA) has a dense branching structure with packed short and long branches.

The chemical structure of PNaAs were confirmed by ATR FTIR (see Figure A4 and Table A1), ^{1}H and ^{13}C NMR spectroscopies as described [19]. L-PNaA - ^{1}H NMR (ppm, D_2O, 300 MHz): δ 2.1 (m, 1H), 0.8-1.7 (m, 2H). $^{13}C\{^{1}H\}$ NMR (ppm, D_2O, 75 MHz): δ 185, 45-47, 36-39. 3-PNaA - ^{1}H NMR (ppm, D_2O with 428 mM NaOH, 300 MHz): δ 3.5-3.6 (m, end group), 3.3-3.4 (m, end group), 2.6 (s, end group), 2.1-2.3 (m, end group), 1.9 (m, 1H backbone), 1.4-1.5 (m, 2H backbone), 1.2 (s, end group), 0.9-1.1 (m, end group). $^{13}C\{^{1}H\}$ NMR (ppm, D_2O with 428 mM NaOH, 75 MHz): δ 185, 170, 67, 58-63, 50, 45-46, 37-39. 28-30, 18. H-PNaA - ^{1}H NMR (ppm, dioxane-d_8, 300 MHz): δ 8.2 (br, branching point), 6.7 (d, end group), 6.5-6.6 (dd, end group), 6.2-6.3 (d, end group), 4.7 (m, branching point and end group), 3.6 (m, branching point and end group), 2.8 (m, 1H backbone), 2.1-2.3 (m, 2H backbone), 1.5-1.7 (m, end group). $^{13}C\{^{1}H\}$ NMR (ppm, dioxane-d_8, 75 MHz): δ 178. 177, 175, 167, 131, 129, 67, 64, 48, 42, 40, 36, 32.

The number-average molar mass (M_n) and dispersity ($D = M_w/M_n$) of L-PNaA were given as 39,300 g/mol and 1.03 respectively. For 3-PNaA and H-PNaA, M_n and D had been determined using size-exclusion chromatography (SEC) in THF after methylation [19] as 8500 and 1.6 respectively for 3-PNaA and 12,300 and 2.2 respectively for H-PNaA. an IUPAC working party has reported that these values, when obtained using SEC, have limited reproducibility and a high uncertainty [25].

We have previously characterised the branching and heterogeneity using free solution capillary electrophoresis in sodium borate at pH 9.2 [19] though their distributions of electrophoretic mobilities. These electrophoretic mobility values also allow the determination of zeta potential [26].

2.2. Cell culture media and conditions

The DLD-1 human adenocarcinoma cell line (ATTC® Number CCL-221™) was acquired from Dr Roger Phillips (University of Bradford, UK) and the ovarian cancer cell lines (A2780/A2780cis) were purchased from Cell Bank Australia™ (ECACC catalogue no. 93112519 and 93112517). All cell lines were grown as monolayer cultures in RPMI-1640 medium with L-glutamine and supplemented with 10 % (v/v) FCS and antibiotics (penicillin 100 IU mL^{-1}, streptomycin 100 mg mL^{-1}). Cell growth using different media are indicated in the figure legends. Cell lines were sub-cultured for a maximum of 20 (DLD-1) or 25 (A2780 and A2780cis) passages. To maintain resistance in the A2780cis sub-cultures, the medium of every third passage was supplemented with 1 μM cisplatin.

2.3. Assessment of cell viability

MTT cell viability assay: Following incubation with drug or polymer, cells were treated with MTT (3-(4,5-dimethylthiazol-2-yl-)-2,5-diphenyltetrazolium bromide) and the number of live cells determined as previously described [27]. The absorbance of control (untreated) wells was assigned a viability of 100 % and the viability of treated wells was expressed as a proportion (%). Cell viability was plotted as a function of polymer or drug concentration, and the cytotoxic potency (IC_{50}) was determined by non-linear regression of a sigmoidal dose-response curve.

SRB assay of cell density: The density of treated cells was assessed using the Sulphorhodamine B (SRB) assay with full details previously published [28]. All absorbance values were corrected by subtracting the background absorbance and the absorbance of the control (untreated) wells was assigned the value of 100 %. Cell survival was expressed as a proportion (%) of total cells relative to control wells and the potency of polymer or drug was determined using the analysis described for the MTT assay.

2.4. Flow cytometry assay for cell cycle analysis

Cell synchronisation, cycle markers and fixation: Following attachment in 6-well plates and recovery from sub-culturing, DLD-1 cells ($2x10^5$) were incubated with serum free RPMI-1640 medium for 24 h to synchronise cells in Gap 0 (G_0) phase [29]. Following synchronisation, cells were incubated in standard conditions in the presence of one of a series of compounds to produce cell cycle arrest in different stages to provide reference points for FACS analysis. Cells were arrested at Gap 1 (G1) phase using Sodium Butyrate (4 mM) [30], in the synthesis (S) phase with Resveratrol (10 μg mL^{-1}) [31], or the mitosis (M) phase with Demecoline (0.1 μg mL^{-1}) [32]. Alternatively, cells were treated with varying concentrations of polymer (10 μg mL^{-1}, 200 μg mL^{-1} or 1000 μg mL^{-1}) for 24 h.

Following incubation, cells were detached by trypsinisation and 10^6 were centrifuged twice for 5 min at 200×*g* with washing in ice cold PBS. The cells were fixed by the dropwise addition of ice cold 'freeze mix' (3:7 ratio 50 mM glycine and absolute ethanol) and stored at −20 °C for at least 24 h to ensure fixation prior to FACS analysis.

FACS Analysis: Cells were centrifuged and resuspended in PBS-T (0.02 % vv^{-1} Tween® 20, 5 mg mL^{-1} BSA in PBS) prior to staining with Propidium Iodide (PI) solution (25 μg mL^{-1} PI, 50 μg mL^{-1} RNase in PBS) in the dark (1 h). PI solution was removed by centrifugation and cells suspended in PBS immediately prior to FACS analysis. PI fluorescence was measured using a BD LSRII Flow Cytometer and *FACSdiva* software (BD Biosciences, NJ, USA), with the PE (λ = 575 nm) laser used for excitation. Debris and doublet cells were gated out and at least 10,000 events were collected per sample. The percentage of cells present within cell cycle stages was determined using *FlowJo v10* (Tree Star Inc, OR, USA) and secondary gating strategies were determined by positive and negative control cells. The gating strategies and distributions with each inhibitor are presented in Figure A1.

2.5. Measurement of apoptosis using the Annexin-V assay

A hallmark feature of intermediate stage apoptosis is the appearance of phosphatidylserine (PS) on the outer leaflet of cells, which is readily detected using FACS with fluorescently labelled Annexin-V. Adherent DLD-1 cells ($2x10^5$) in 6-well plates treated with cisplatin (13.5 μM) for 24 h provided a positive control for apoptosis and necrotic control cells were produced with ethanol (30 % vv^{-1}, 2 h). The ability of PNaA to elicit apoptosis was assessed with varying concentrations of polymer (10 μg mL^{-1}, 200 μg mL^{-1} or 1000 μg mL^{-1}) for 24 or 72 h prior to analysis and unstained control cells were incubated in RPMI-1640 medium for equivalent times.

Cells harvested by trypsinisation were washed and suspended in 100 μL Annexin-V Binding Buffer (10 mM HEPES, 150 mM NaCl, 5 mM KCl, 2 mM $CaCl_2$ in water) as previously described [33]. Annexin V-FITC (0.375 μg mL^{-1}) was added to all samples and incubated in the dark at 20 °C for 10 min. Cells were suspended in Annexin–V Binding buffer (200 μL) and stained with PI (5 μg mL^{-1}) immediately prior to FACS analysis. Apoptotic positive cells were only incubated with Annexin V-FITC and the necrotic positive cells were only incubated with PI.

FACS based detection of apoptosis and cellular necrosis were identified by staining with two different stains, Annexin V-FITC and PI using the 488 nm and 575 nm (PE) lasers for excitation. Colour compensation was required because FITC and PI have overlapping emission spectra and the optimal gating strategy provided in Figure A2. Compensation was set up at the start of each experiment and used to set secondary gates, with at least 10,000 events (single cells) collected for all channels (brightfield, Annexin-V-FITC and PI). Flow cytometry data were collected with the BD LSRII Flow Cytometer using *FACSdiva* Software (BD Biosciences, NJ, USA) and analysed using *Flowjo v10* software (Tree Star Inc, OR, USA).

2.6. Cargo loading of PNaA with cisplatin and measurement of Pt content using ICP-MS

Cargo loading of PNaA: The anticancer drug cisplatin was loaded onto PNaA by virtue of the pH-dependent ionisation properties of the polymer (Figure A5). Linear PNaA (1.44 mg mL^{-1}) was dissolved overnight in water leading to a ~pH 9 solution. Branched PNaAs in their acid form (1.44 mg mL^{-1}) were suspended overnight in water and the pH was raised to ~pH 9 with NaOH. Cisplatin (2.5 mg mL^{-1}) was added and samples vortexed for 5 min then incubated at 25 °C for 72 h, with further vortexing every 24 h. The alkaline pH was maintained by the addition of NaOH every 24 h. Following incubation, the samples were dialysed using a molecular weight cut-off <1000 for 24 h at 20 °C. Conjugation was confirmed by capillary electrophoresis (CE), see below for details, and the dialysed conjugated samples were stored at 6 °C until used.

Measuring cargo loading on PNaA: The amount of platinum (from cisplatin) loaded onto PNaA was measured with inductively coupled mass spectrometry (ICP-MS). Prior to ICP-MS analysis, the loaded polymer (PNaA-Pt) samples were digested in a mixture of concentrated aqueous hydrochloric acid (HCl) and nitric acid (HNO_3) (1 part HCl to 9 parts HNO_3). Platinum concentrations were determined using a NexION 200 Inductively Coupled Plasma Mass Spectrometer (ICP-MS, PerkinElmer) programmed to detect $Platinum^{195}$ and calibrated with external standards (0.4, 1, 10, 50 and 100 ppb). Technical staff in the Mass Spectrometry Facility in the Department of Chemistry, University of Sydney, undertook ICP-MS analysis of the digested polymer samples.

2.7. Capillary electrophoresis of PNaA

The physical properties and cargo loading of PNaA were measured using free-solution Capillary Electrophoresis (CE). All separations were performed using a 7100 CE system (Agilent Technologies, Germany) with a fused silica capillary (Polymicro, United States) of 50 μm internal diameter, a total length of 62 cm and an effective length of 53.5 cm in 110 mM sodium borate buffer at pH 9.2. Conditions for CE separation were validated using an oligoacrylate standard (AA4) of known electropherogram as previously described [34,35]. DMSO (0.2 % vv^{-1}) was used as an electroosmotic flow (EOF) marker and data was collected at λ = 195 nm with a bandwidth of 10 nm. Capillary preconditioning, injection conditions and run parameters have been previously described [19]. Data was acquired using *ChemStation A.10.01* software and analysed with *Origin 9.5* software. Calculation of μ and the dispersity value of μ distributions were previously described [26].

2.8. Preparation of fluorescently tagged PNaA

The chemistry of PNaA allows both the reversible attachment of cargo such as drugs, and the covalent grafting of moieties for detection or targeting applications. A two-step chemical reaction using two coupling reagents to attach the fluorescent compound BODIPY FL to PNaA is shown in Figure A6. The coupling agents *N*-hydroxysuccinimide (NHS) (20.37 mg mL^{-1}) and 1-ethyl-3-(3-dimethylaminopropyl) carbodiimide hydrochloride (EDC-HCl) (1.51 mg mL^{-1}) were dissolved in water directly prior to use and BODIPY® FL EDA was dissolved in DMSO (3.7 mg mL^{-1}) and stored at −20 °C. PNaA and coupling agents were combined such that the carbodiimide of EDC-HCl reacted with carboxyl moieties on PNaA resulting in an unstable *O*-acylurea ester intermediate (3-(((ethylamino-(hydroxy)methylene)amino)-*N*,*N*-dimethylpropan-1-amine (EDH)). The unstable *O*-acylurea intermediate undergoes nucleophilic substitution with a stable NHS-ester activating the carboxyl group of PNaA. The NHS-ester species reacts (for 24 h, 20°C in the dark) with the primary amine of BODIPY™ FL EDA and leaves, thereby facilitating the covalent attachment of BODIPY™ FL EDA to PNaA. The final product, aiming at 1 BODIPY substituent per macromolecule, was dialysed (molecular weight cut-off <1000) for 24 h at 20 °C with several buffer changes, protected from light and subsequently stored at 4 °C

until use.

2.9. Fluorescence microscopy for tagged PNaA

The cellular uptake of $PNaA^{BODIPY}$ was assessed using fluorescent microscopy and co-stained with the nuclear marker Hoechst 33342. Cells were washed with PBS to remove traces of RPMI-1640 and replaced with phenol red free DMEM. Cells were incubated for 15 min with $PNaA^{BODIPY}$ (1000 μg mL^{-1}) at 37 °C with 5 % CO_2. Following incubation, the cells were washed with PBS to remove $PNaA^{BODIPY}$ and incubated with Hoechst 33342 (1:1000 ratio) for 10 min at 37 °C with 5 % CO_2. The cells were mounted in ProLong™ Diamond Antifade Mountant (ThermoFisher Scientific), sealed with a 1.5 thickness coverslip and slides stored at 37 °C until imaging. Images were acquired using the Zeiss LSM800 Airyscan (Carl Zeiss, Jena, Germany) with an Axio Imager Z2 upright microscope with a 63x1.4 NA lens. Two tracks were used simultaneously with bright field detection (*Track One*: BODIPY™ FL EDA detection, excitation: 488 nm, detection range: 500-575 nm, *Track Two*: Hoechst 33342 detection, excitation: 405 nm, detection range: 400-500 nm, bright field detection wavelength of 400-500 nm).

2.10. Statistical analyses

Data are presented as mean ± standard error of the mean (SEM) for the indicated number of independent experiments. Statistical evaluations comparing the mean values of two parameters used the Student's t-test. Multiple ($n \geq 3$) comparisons used a one-way ANOVA, employing a Dunnett's or a Tukey's *post-hoc* test. A P value of <0.05 was considered statistically significant. Graphical representations of data used GraphPad Prism® Software v5 (CA, USA) and where required, were analysed with non-linear least squares regression.

3. Results

3.1. Toxicity profile - the effects of PNaA addition on cell cycle distribution of cultured cancer cells

Several distinct assays were used to determine whether PNaA elicited inherent toxicity using the well characterised DLD1 colon adenocarcinoma cell line provided as a model system. The initial strategy was to determine whether PNaA altered progression through the cell cycle using flow cytometry with the nuclear stain PI.

Fig. 1 compares the phase distribution of DLD1 cells in the presence or absence of free cisplatin and the data are expressed as a proportion of total cell population. Cisplatin treatment provided a positive control for cell cycle disruption as seen by the significant increase in the pre-G_0 population (sub-G_0), with a concomitant reduction in the proportion of cells in G_0/G_1, S and G_2/M phases. The sub-G_0 population reflect cell debris or cell remnants, thereby indicating widespread cytotoxicity caused by cisplatin.

The cell cycle distribution profiles compared to untreated controls are shown in Fig. 2 following the administration of all three branching topologies of native PNaA (three concentrations) to DLD1 cells (two time periods). There were no significant alterations in the cell cycle distribution following a 1-day incubation with PNaA compared to untreated control, regardless of the concentration of polymer used. In contrast, a 3-day incubation of polymer with DLD-1 cells produced a dose-dependent increase in the pre-G_0 population of cells, however, the effect was primarily confined to the high concentration (i.e. 1000 μg ml^{-1}). At this high concentration of polymer administered over three days, the proportion of cells in G_0/G_1, S and G_2/M phases were marginally reduced.

In summary, although PNaA produced cell cycle disruption to DLD-1 cells, the effect was only significant at the highest concentration used and this is likely to exceed the amounts used to deliver cisplatin. Moreover, the effects were only apparent following a prolonged exposure of cells to the polymer.

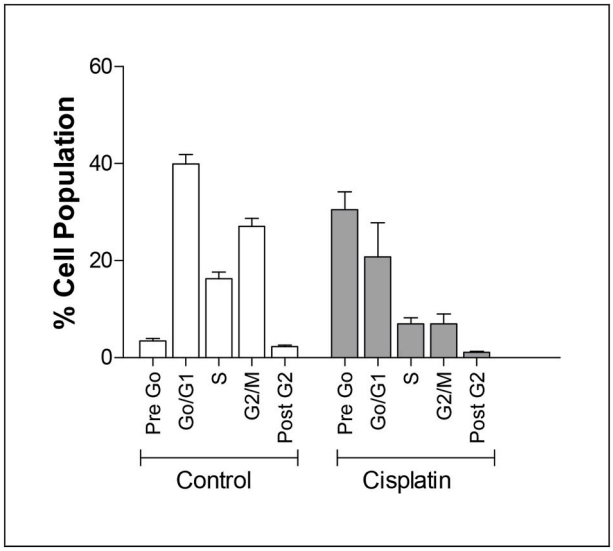

Fig. 1. Cell cycle analysis following administration of cisplatin.
DLD1 cells were treated with cisplatin (13 μM) for 6 h and subsequently incubated 24 h in drug free culture medium for 24 h to recover. Flow cytometry analysis was used to compare the distribution through the cell cycle either treated or not treated with cisplatin. Prior to treatment, the cells were synchronised to G_0-phase as described in the methods. All values represent the mean ± SEM obtained from three independent observations.

3.2. Toxicity profile – effects of PNaA addition per se on apoptosis in cultured cancer cells

The effects of PNaA on cell-cycle distribution were predominantly an increase in the pre-G_0 phase, but this crude toxicity marker does not discriminate between an apoptotic response and a necrotic effect. Consequently, the ability of PNaA to elicit an apoptotic response was measured in DLD-1 cells using an Annexin-V assay that measures the appearance of PS in the outer leaflet of cell membranes.

The three topologies of PNaA were administered to DLD-1 cells at different concentrations for a period of 1 (Fig. 3a–c) or 3 days (Fig. 3d–f) and compared to untreated controls and to cells incubated with cisplatin (13.5 μM). In all cases, the addition of cisplatin significantly increased the number of early apoptotic cells to between 25 and 30% of the population. No late apoptotic or necrotic cells were detected following cisplatin treatment under any of the conditions used.

Addition of L-PNaA and H-PNaA for 1-day produced comparatively smaller increases in the proportion of early apoptotic cells, but only at the highest concentration of 1000 μg ml^{-1}. These topologies of PNaA also resulted in the detection of late apoptotic cells, albeit at less than 5% of the population. Administration of the 3-PNaA polymer topology (Fig. 3b) over a 1-day period resulted in increased levels of early apoptotic cells in a concentration dependent manner.

In a manner similar to the observations on cell cycle distribution, the 3-day incubation of DLD-1 cells with PNaA produced the most sizable response. In particular, treatment of cells with the 3-PNaA and H-PNaA topologies increased the proportion of early apoptotic cells, accounting for >10% of the cell population, but this was restricted to concentrations of 1000 μg ml^{-1}. In contrast, there were no significant increases in the proportion of apoptotic cells at any of the L-PNaA concentrations used.

None of the polymers, under any condition, produced an increase in the number of necrotic cells and indicated a programmed apoptotic response. It is noteworthy that apoptotic cells were only produced at the highest concentration used and the effects were most prominent following a prolonged 3-day incubation, thereby demonstrating the

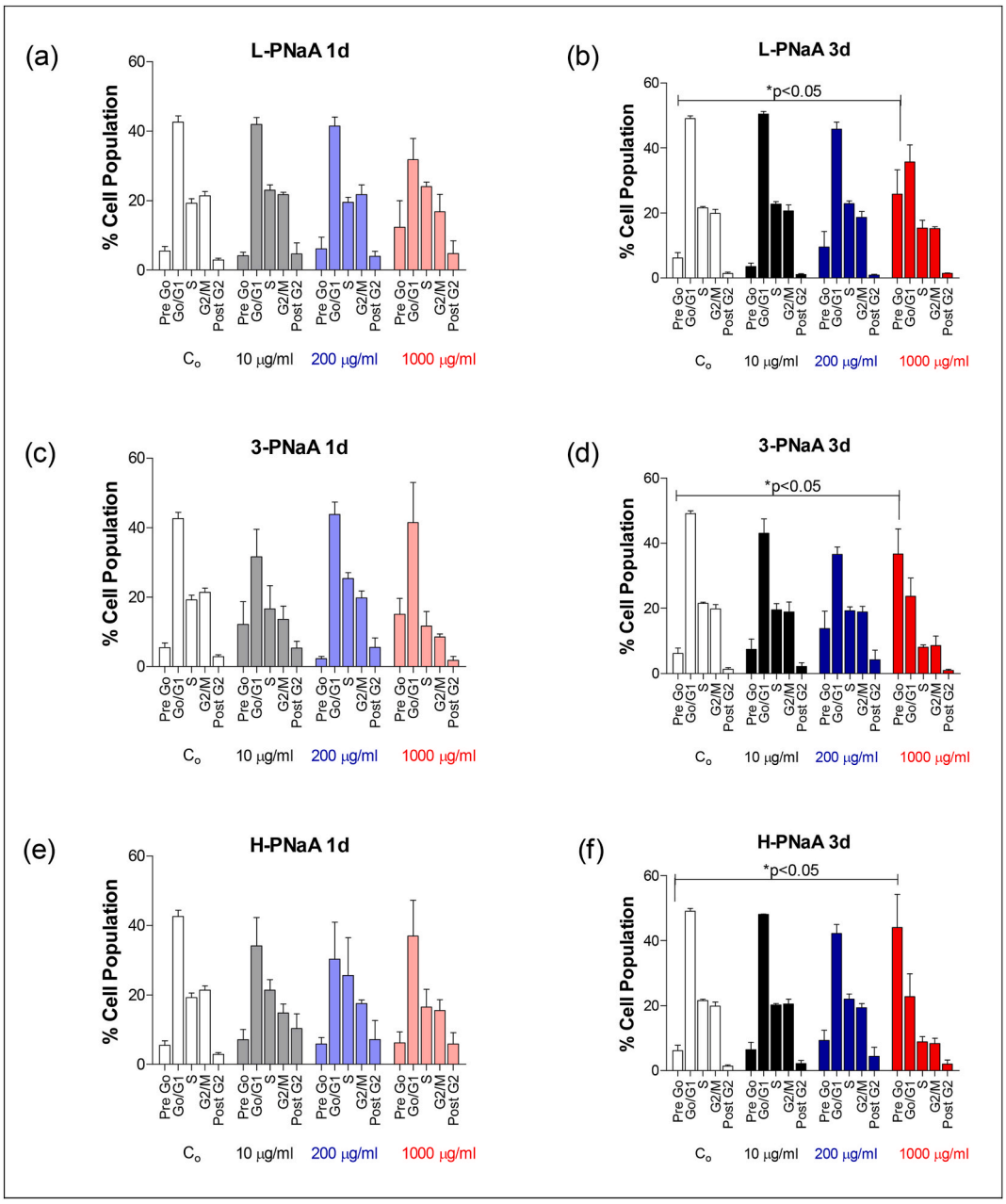

Fig. 2. Cell cycle analysis following administration of various topologies of PNaA.
The three topologies of PNaA were administered to DLD1 cells for 1 (a, c, e) or 3 (b, d, f) days. C_o refers to cells treated with the vehicle control. PNaA topologies were administered at concentrations of 10 (grey bars), 200 (blue bars) or 1000 (red bars) μg polymer/ml culture medium. Flow cytometry analysis was used to compare the distribution through the cell cycle following the respective treatments. Prior to treatment, the cells were synchronised to G_0-phase as described in the methods. All values represent the mean ± SEM obtained from three independent observations. (For interpretation of the references to colour in this figure legend, the reader is referred to the Web version of this article.)

biological compatibility of PNaA.

3.3. *Toxicity profile – effects of drug-free PNaA on the proliferation of cultured cancer cells*

Our ultimate objective is to demonstrate whether cisplatin loaded onto PNaA produces an anti-proliferative effect greater than the drug alone. Prior to assessing the efficacy of the PNaA-cisplatin complex, it is important to assess whether the polymer *per se* can impair cell proliferation.

The ability of each native PNaA topology to alter cell growth was measured using an SRB staining procedure that reports the total cell number (Fig. 4). Cisplatin was again used as a positive control and inhibited cell proliferation at concentrations in the low micromolar range. Polymer topologies (10-1000 μg ml^{-1}) were added to cells for a prolonged 3-day incubation, followed by a 3-day recovery period prior to cell staining. Each of the topologies inhibited cell proliferation and their IC_{50} values are shown in the respective panels. The IC_{50} values ranged between 700 and 850 μg ml^{-1}, which is broadly consistent with the observations that only high concentrations of PNaA produced effects on cell cycle distribution and apoptosis.

Overall, the results demonstrate that native PNaA can alter cell proliferation; however, this only occurs following prolonged incubation times and at high polymer concentrations. Delivery of cisplatin to

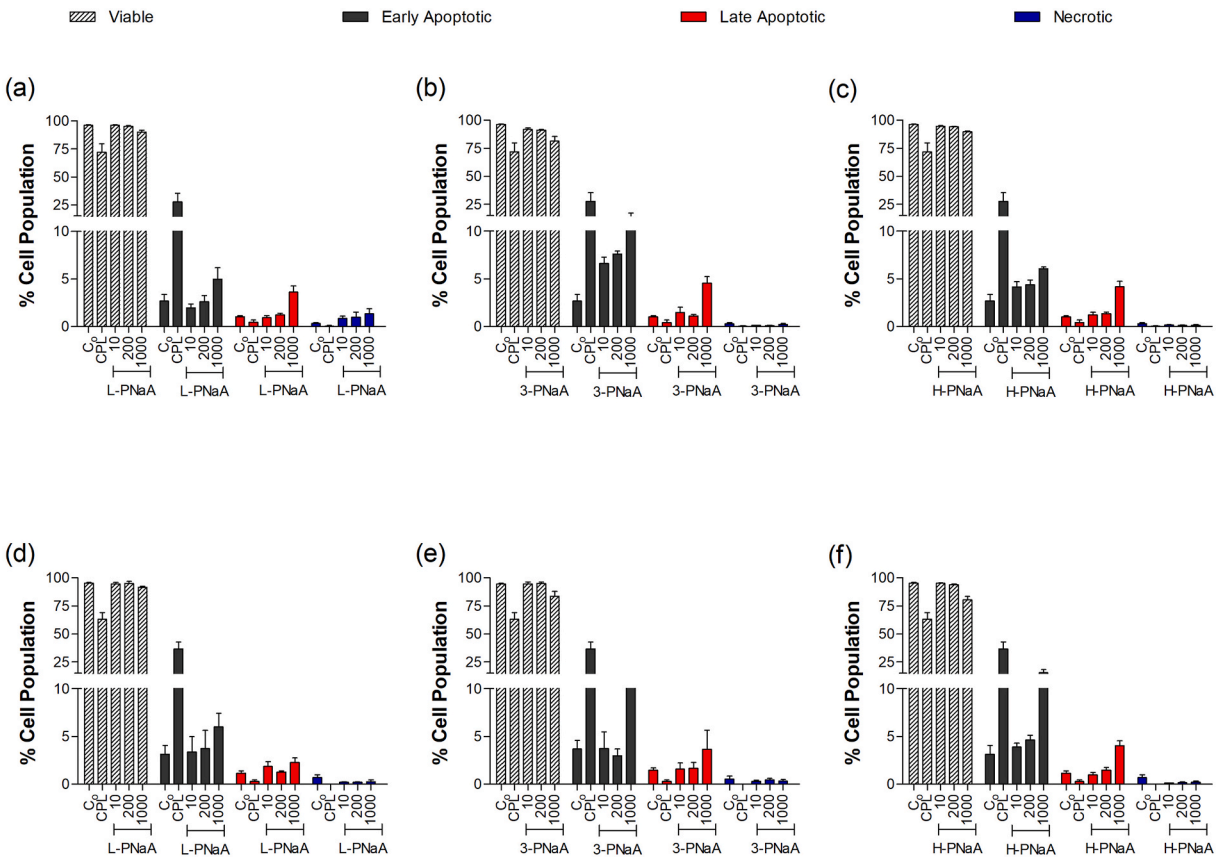

Fig. 3. Initiation of apoptosis in DLD1 cells by administration of PNaA.
DLD1 cells were treated with one of three topologies of PNaA for either 1 (a-c) or 3 (d-f) days at concentrations of 10, 200 or 1000 μg polymer/ml culture medium. C_o refers to untreated control cells and CPL indicates cell treatment with 13 μM cisplatin. The distribution of viable, early apoptotic, late apoptotic or necrotic cells was determined by flow cytometry using an Annexin-V FITC kit. All values represent the mean ± SEM obtained from three independent observations.

produce extensive cytotoxicity is unlikely to use the concentrations of polymer capable of eliciting inherent cytotoxicity.

3.4. Loading of cisplatin cargo onto linear and complex topologies of PNaA

Loading of cisplatin to PNaA does not require alteration of the polymer's chemical structure and makes use of the pH-dependent changes in ionisation state of the polymer. At pH 9, PNaA contained ionised carboxylic acid side-chain moieties that bound cisplatin following displacement of its chloride ions.

To verify the attachment of cisplatin, dialysed PNaA was analysed by CE and the results shown in Fig. 5(a–c). CE provides a rigorous and well-established analytical method for polymer-cargo assessment by virtue of mobility shifts as highlighted [36]. Native, or empty, L-PNaA was characterised by a narrow and sharp peak (Fig. 5a) with electrophoretic mobilities between 3.5 and 4.0 x 10^{-8} m^2 V^{-1} s^{-1} as previously determined [26]. The branched 3-PNaA and H-PNaA topologies were characterised by a sharp, narrow peak superimposed on a broader underlying peak (Fig. 5b–c), in agreement with previous observations [19]. Following attachment of cisplatin, all three polymer topologies displayed marked alterations to their mobility patterns in CE. The decreased electrophoretic mobility and broad shape were associated with a reduced charge due to the loss of unbound carboxylate moieties and an increase in hydrodynamic friction. The increase in dispersion (broadness) indicates a heterogeneous composition of PNaA resulting from the successful attachment of cisplatin. However, cisplatin does not attach to the same positions on different PNaA macromolecules. The large increase in peak area between native and loaded PNaAs is consistent with the loading of cisplatin and the higher Beer-Lambert (UV absorption) coefficients of platinum compounds compared to PNaA.

Quantitative validation for the attachment of cisplatin to PNaA was achieved using ICP-MS, which detects the presence of metals, in this case platinum. The approach has been validated for numerous metal compounds including platinum [37,38]. PNaA samples with attached cisplatin were digested with nitric and hydrochloric acids prior to ICP-MS analysis and Fig. 5d shows the amount of platinum incorporated per unit measure of polymer. L-PNaA incorporated 4.3 ± 0.4 μmol Pt g^{-1} polymer, with higher incorporation of platinum observed in the 3-PNaA and H-PNaA polymer topologies 5.4 ± 0.3 and 5.3 ± 0.1 μmol Pt g^{-1} ($p < 0.05$) respectively.

In summary, two distinct methods demonstrated that cisplatin could be readily attached to all three topologies of PNaA. Additionally, the measured loading capacities of platinum were used to determine the amount of cisplatin delivered by polymer in subsequent investigations. This allowed for a quantitative comparison of cytotoxicity parameters relative to the addition of free cisplatin.

3.5. The relative anti-proliferative efficacy and potency of cisplatin compared to cisplatin-loaded PNaA in culture cancer cells; the influence of pH

PNaA is classified as a smart polymer with a release mechanism for its cargo that is pH-dependent. In particular, the release of cargo from PNaA is triggered by acidic conditions, thereby rendering it ideal for the acidic microenvironment common to solid tumours. To test this hypothesis, the cytotoxicity of PNaA loaded with cisplatin (Pt-PNaA) on cancer cells was measured at multiple pH-values between 6.0 and 7.5.

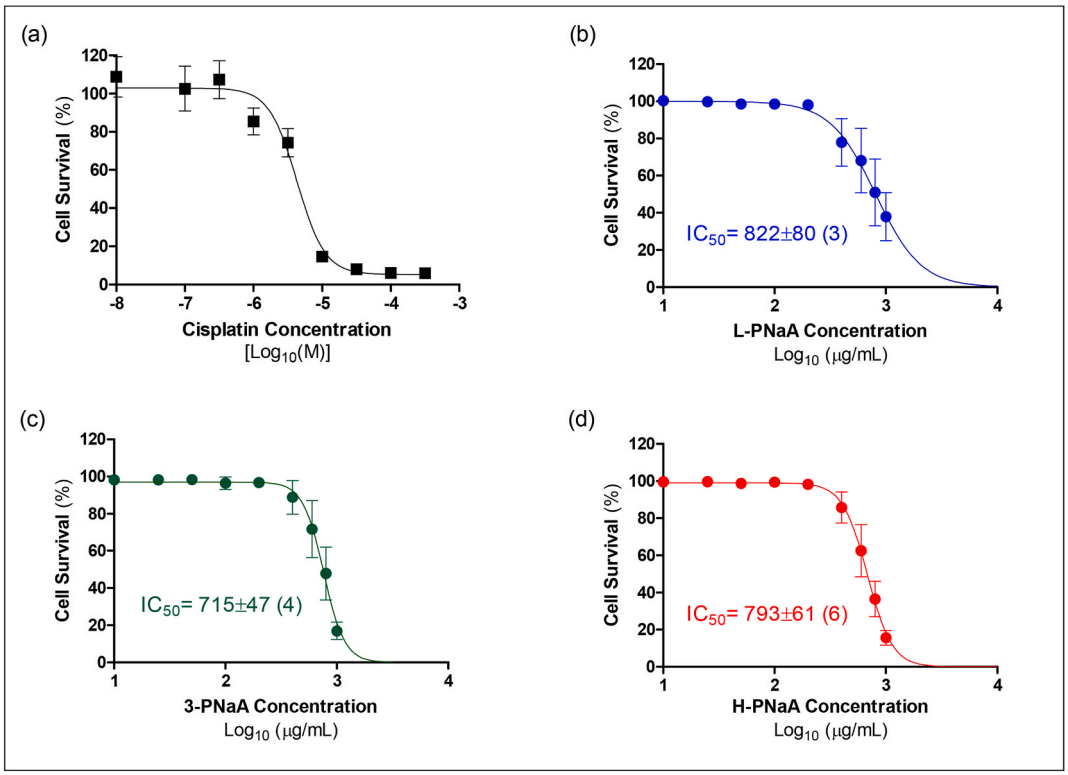

Fig. 4. The effects of PNaA administration on the survival of DLD1 cells.
DLD1 cells were treated for (a) 6 h with cisplatin or for 72 h with (b) L-PNaA, (c) 3-PNaA or (d) H-PNaA and subsequently allowed to recover for 72 h in the absence of drug or polymer. Cell survival following treatment was measured using the SRB-assay described in the methods and plotted as a function of concentration. The IC_{50} values for inhibition of cell survival were determined by non-linear regression of the general dose-response relationship. Values in the figures provide the mean ± SEM corresponding to the number of independent observations indicated in parentheses.

This is the maximal range of pH in culture medium that maintain the viability of cells up to 6 h (*data not shown*).

The effects of free cisplatin (1 h incubation, 24 h recovery) on DLD-1 cell growth at several pH values between 6.0 and 7.4 (Fig. 6a) provided a reference for the ensuing measurements with Pt-PNaA. Neither the potency of cisplatin to inhibit DLD-1 proliferation, nor the extent of the cytotoxic response were affected by changing the pH of the culture medium. Cytotoxicity profiles were generated in DLD1 (Fig. 6b) and A2180 (Fig. 6c) cells for each of the Pt-PNaA topologies at pH 7.4 and compared to free cisplatin. The concentrations of cisplatin loaded PNaA were related to the amount of Pt bound to the polymer and are referred to as the effective cisplatin concentration. The same dose-response relationships were done at multiple pH conditions and the IC_{50} values for cytotoxicity obtained by non-linear regression. Table 1 summarises the data obtained for DLD-1 cells, while Table 2 presents the data for A2780 (drug-sensitive) and A2780cis (cisplatin-resistant) cells. Cells were exposed to free, or polymer-attached, cisplatin for 1 h followed by a 24-hr recovery period prior to the MTT assay for cell proliferation. The short exposure time to polymer was chosen to ensure negligible inherent cytotoxicity of native PNaA to the cell lines.

The most striking observation in DLD-1 cells was the dramatic increase in the potency of cisplatin to produce cytotoxicity when attached to PNaA (Table 1). The increase in potency compared to free cisplatin ranged from 1343-fold with the hyperbranched polymer to 2704-fold with the linear topology. The rank order to improve the potency of cisplatin by the three topologies was L-PNaA-Pt > 3-PNaA-Pt > H-PNaA-Pt. This is in contrast to data shown in Fig. 4, which demonstrated no potency differences between the three topologies of drug free PNaA. Another significant, but somewhat surprising, observation was that regardless of topology, the potencies of Pt-PNaA were unaffected by adjusting the culture medium pH in the range 6.0-7.4. This observation is surprising since the reduction in pH would be expected to release cisplatin from the polymer and thereby enhance its cytotoxic efficacy.

The effects of pH on the cytotoxicity of all three Pt-PNaA topologies were also measured in the A2780 ovarian cell line and its cisplatin resistant variant, A2780cis. The data are shown in Table 2 and the effects of free cisplatin once again used as a control. The IC_{50} for cisplatin to produce cytotoxicity in A2780 cells (391 ± 32 μM) was 3.7-fold lower than that observed in A2780cis cells, thereby demonstrating the resistant phenotype in the latter. In addition, the IC_{50} value in A2780 cells was markedly lower than observed in DLD-1 cells which may indicate a relative insensitivity of colon cancer tissue to cisplatin. Attachment of cisplatin to PNaA (regardless of topology) produced a significant increase in the potency to generate a cytotoxic response in both A2780 and A2780cis cells. However, adjusting the culture medium pH (7.4 to 6.0) did not alter the IC_{50} values to elicit cytotoxicity in either the A2780 or A2780cis lines. This is analogous to observations with the DLD1 cells and suggests a pH-independent mechanism of cisplatin release.

In summary, the attachment of cisplatin to PNaA inhibited the proliferation of cancer cell lines and with a markedly higher potency than observed using free drug. The improved potency was observed with the linear, 3-arm star and hyperbranched versions of PNaA; however, the linear form provided the most benefit. Our original mechanism of action suggested that lowering the pH from 7.4 to 6.0 would provide further improvement since the acidic environment was expected to trigger cisplatin release from the polymer and produce a higher local concentration of the drug. This was not the case under the conditions used, suggesting an alternative mechanism of cisplatin delivery by PNaA.

3.6. *Cisplatin release from the three topologies of PNaA*

Our assumption is that cisplatin attachment to PNaA is reversible and

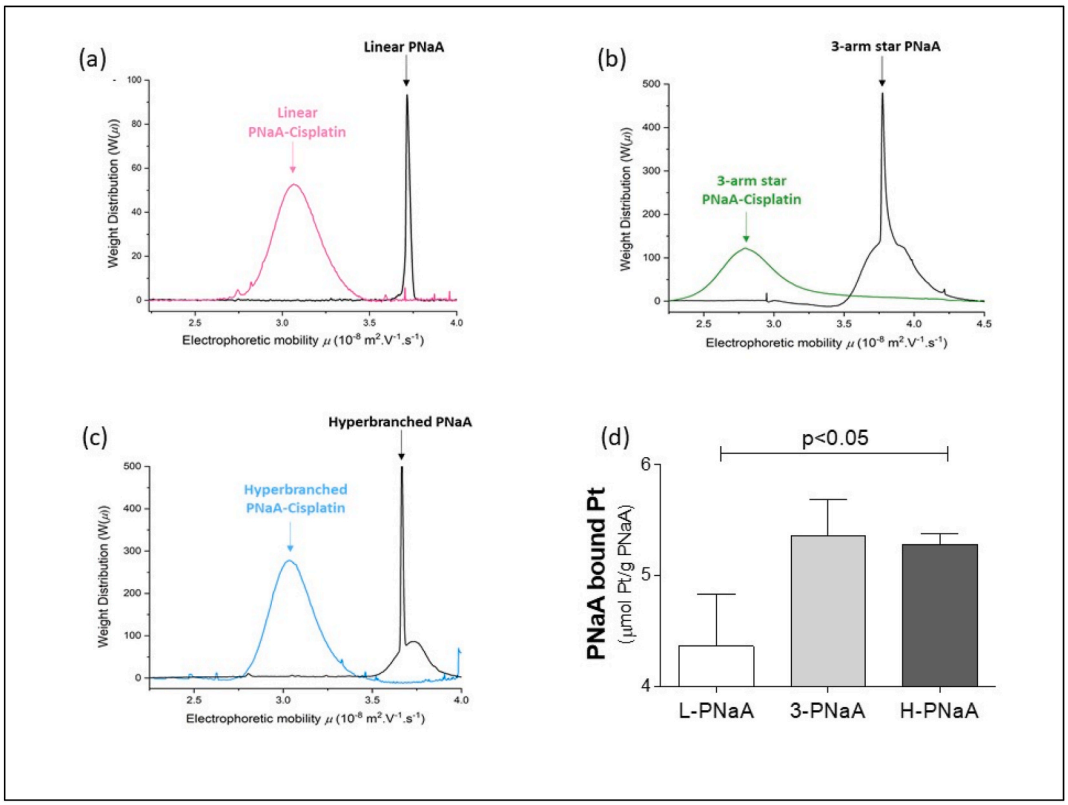

Fig. 5. Loading the three toologies of PNaA with cisplatin.
All PNaA topologies were loaded with cisplatin for 72 h as described in the methods and dialysed prior to analysis by CE. Distributions of electrophoretic mobilities are shown for (a) L-PNaA, (b) 3-PNaA and (c) H-PNaA in their empty (*black*) and post-loading (*coloured*) states. Panel (d) shows the amount of platinum loaded onto each polymer topology and was measured using ICP-MS analysis. Values represent the mean ± SEM corresponding to the number of independent observations indicated in parentheses.

following the release of drug the polymer will revert to the characteristic electrophoretic mobility of unlabelled PNaA.

Electropherograms of L-PNaA, 3-PNaA and H-PNaA shown in Fig. 7 display their distributions of electrophoretic mobilities in unlabelled and labelled forms under a variety of pH conditions, in addition to the mobility of labelled polymer in water as a reference. The PNaA-Pt profiles are provided at the start (*first injection*) and the end (*last injection*) of an extended 12-24 h incubation period. As expected, the mobility of PNaA-Pt was significantly reduced compared to the corresponding unlabelled polymer. However, the peak shape also varied between pH conditions. For example, the profiles for L-PNaA-Pt and H-PNaA-Pt (*panels D-E*) were markedly broader than observed for 3-PNaA-Pt (*panel B*) in the same buffer environment (pH7.4). The differences in peak shape likely represent the varying apparent charge properties of the polymer under different pH-conditions and the variability is exacerbated by the distinct conformations.

The mobility of 3-PNaA-Pt and L-PNaA at the end of the incubation period shifted towards the mobility observed for unlabelled 3-PNaA (*panels A-C*) and L-PNaA (panel D) and reflects a partial reversion following cisplatin release. The shift in mobility is not observed for H-PNaA at pH 6.0 and it is very limited if significant at high pHs (panel E). The incubation periods corresponded to 12-hr and an extension to 24-hr failed to result in full recovery to the mobility of PNaA. The CE data demonstrated that PNaA is able to release cisplatin under a variety of buffer conditions and that L-PNaA and 3-PNaA appears to show the greatest propensity to release cisplatin, presumably due to their comparatively simple architecture. However, the observed release remained partial over an extended 12-24 h period, regardless of the polymer topology. This slow and partial release of cisplatin contrasts with the marked and potent effects of Pt-PNaA on cell proliferation obtained after only a 1-hr incubation with cells. The anti-proliferative effect of Pt-PNaA in the absence of substantial extracellular release of cargo may imply an alternative mechanism to our initial hypothesis.

3.7. *Developing a fluorescent derivative of PNaA to assess its cellular interaction*

The likely alternative mechanism of cytotoxicity involves the uptake of the whole Pt-PNaA complex by cells prior to extensive intracellular dissociation of drug. In order to investigate this mechanism, we required an approach to detect the polymer and establish its intracellular localisation. Consequently, a fluorescent derivative of PNaA was synthesised to detect the polymer using microscopy analysis.

Details of the procedure to graft the fluorescent BODIPY FL moiety to PNaA using coupling agents are provided in the methods section and a schematic provided in Figure A6. Following extensive dialysis to remove unbound BODIPY FL, a fluorescence emission scan was done with labelled and unlabelled PNaA as shown in Fig. 8a. All three topologies of $PNaA^{BODIPY}$ were characterised with an emission maximum at 510 nm and fluorescence intensities in the range 272-328 r.f.u. In contrast, native PNaA topologies that had not undergone chemical modification to attach BODIPY FL exhibited negligible fluorescence between 500 and 600 nm. Unattached BODIPY FL was characterised with an emission maximum at 520 nm and low intensity.

The fluorescence data indicate the covalent attachment of BODIPY to PNaA and this observation was validated further with CE. As shown in Fig. 8b, native L-PNaA migrated with a mobility at peak maximum of 3.8 x 10^{-8} m^2 V^{-1} s^{-1} and a peak intensity of 151 arbitrary units. Attachment of BODIPY-fluorophore caused a marked shift in the electropherogram, with $PNaA^{BODIPY}$ migrating with a mobility of 3.2 x

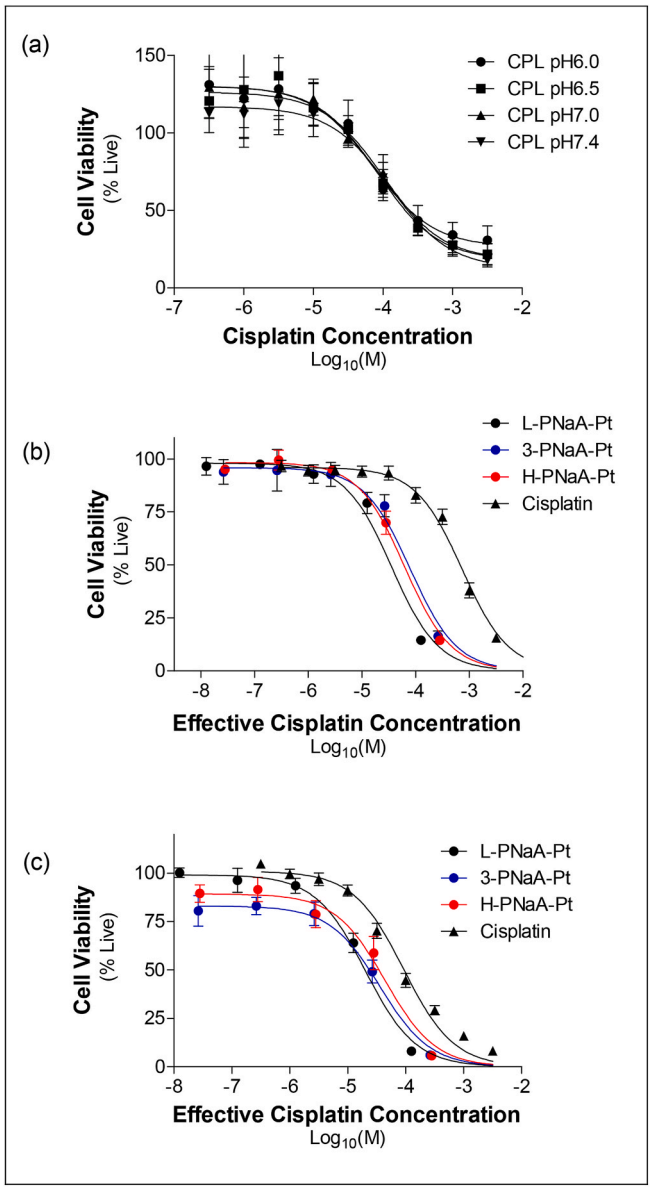

Fig. 6. Cytotoxicity of cisplatin loaded PNaA to DLD1 and A2780 cells (a) The cytotoxicity of cisplatin to DLD1 cells was measured at the indicated pH values between 6.0 and 7.5 following a 1 h drug exposure and a 24-hr recovery period. (b) The cytotoxicity of PNaA loaded with cisplatin was compared to free drug at pH7.4 using RPMI medium with DLD1 cells. The three topologies of loaded polymer, and cisplatin, were incubated with cells for 1 h, followed by a 24-hr recovery period in medium. (c) Identical treatment regime to panel (B) with the A2780 cell line.
The cell viability was measured colorimetrically using the MTT assay and all values indicate the mean ± SEM obtained from at least three independent observations. Cell viability was plotted against concentration. In the case of loaded polymer, the effective cisplatin concentration was determined from the amount of platinum loaded (measured by ICP-MS).

10^{-8} m^2 V^{-1} s^{-1} and a peak intensity that was increased 36-fold to 5470 arbitrary units. Chemical modification resulted in altered mobility of $PNaA^{BODIPY}$ in CE due to decreased charge and increase hydrodynamic friction compared to PNaA.

Data from fluorescence spectroscopy and CE demonstrate the successful covalent attachment of BODIPY FL to PNaA. The resultant $PNaA^{BODIPY}$ may be detected in a cellular environment and enable us to ascertain whether it is internalised by cells.

Table 1
Cytotoxicity of cisplatin conjugated to PNaA at different pH values in DLD1 cells.

AGENT	pH	IC_{50} (μM)	Fold Increase
CPL	7.4	1893 ± 131 *(40)*	n/a
L-PNaA	6.0	0.66 ± 0.18 *(6)*	2686
	6.5	0.32 ± 0.01 *(6)*	5916
	7.0	0.65 ± 0.09 *(6)*	2912
	7.4	0.70 ± 0.09 *(6)*	2704
3-PNaA	6.0	1.25 ± 0.21 *(7)*	1514
	6.5	1.47 ± 0.25 *(7)*	1288
	7.0	1.33 ± 0.27 *(7)*	1423
	7.4	1.08 ± 0.21 *(7)*	1753
H-PNaA	6.0	1.50 ± 0.29 *(7)*	1262
	6.5	1.52 ± 0.33 *(7)*	1245
	7.0	1.44 ± 0.16 *(7)*	1315
	7.4	1.41 ± 0.24 *(7)*	1343

The three PNaA topologies were loaded with cisplatin and added to culture media at the specific pH values indicated. The pH values in culture medium (bicarbonate-free) were maintained with a phosphate buffer system. Exposure to PNaA-Pt (or free cisplatin as a control) was for 1 h and then permitted to recover for 24 h prior to the MTT assay on cell viability. The IC_{50} value to produce cytotoxicity was determined by regression of the general dose-response relationship. The Fold-Increase parameter refers to the improvement in potency (IC_{50}) afforded by the PNaA-Pt topologies compared to free cisplatin. All values refer to the mean ± SEM obtained from the number of independent observations indicated by the parentheses.

3.8. Uptake and intracellular distribution of PNaA in cultured cancer cells

Polymeric nanoparticles may be internalised by cells through one of the endocytic pathways and in general, the upper limit for internalisation is a radius of 60 nm [39,40]. The three PNaA topologies used in this manuscript have hydrodynamic radii <5 nm [18], which renders them susceptible to internalisation via endocytosis. Dimensions are not the sole driver for internalisation, which is also influenced by surface properties such as charge and hydrophobicity.

DLD-1 cells were incubated with high concentrations (1000 μg ml^{-1}) of $PNaA^{BODIPY}$ for 15 min and counter stained with the nuclear dye Hoechst 33342. Fig. 9 (*column iii*) shows the appearance of intracellular $PNaA^{BODIPY}$ that is primarily localised within the cytoplasm of DLD-1 cells. Cytoplasmic localisation of $PNaA^{BODIPY}$ within 15 min was observed for the linear (*row a*), 3-arm star (*row b*) and hyperbranched (*row c*) topologies of polymer and included a punctate appearance (*white arrows*). The dual stain, or merged, images (*column iv*) indicate that many of the punctate stains are localised within the cytoplasm at the perinuclear region and there is evidence for nuclear penetration (*orange arrows*). Images obtained using confocal microscopy provided optical sectioning of DLD-1 cells at 1 μm intervals to provide 3-D information. The side-by-side views in Figure A7 suggest nuclear penetration of 3-$PNaA^{BODIPY}$ and H-$PNaA^{BODIPY}$ rather than surface adsorption. However, the intra-nuclear accumulation of $PNaA^{BODIPY}$ represents a small proportion of the total fluorescence and likely due to leakage from the perinuclear location.

In summary, all three topologies of PNaA rapidly enter DLD-1 cells and show punctate accumulation predominantly at the perinuclear region. This perinuclear staining pattern is suggestive of lysosomal accumulation, which is the cellular destination for endocytic vesicles. Based on the slow time-course of cargo release from PNaA (see Fig. 7), we propose that the anti-proliferative efficacy of Pt-PNaA (*see* Fig. 6, Tables 1 and 2) is elicited following the cytoplasmic accumulation of

Table 2
Cytotoxicity of cisplatin conjugated to PNaA at different pH values in A2780 and A2780cis cells.

		A2780		A2780cis	
AGENT	pH	IC_{50} (μM)	Fold Increase	IC_{50} (μM)	Fold Increase
CPL	7.4	391 ± 32 *(42)*	n/a	1439 ± 142 *(14)*	n/a
L-PNaA	6.0	0.43 ± 0.11 *(6)*	912	0.96 ± 0.187 *(3)*	1499
	6.5	0.45 ± 0.09 *(6)*	933	1.20 ± 0.16 *(3)*	1199
	7.0	0.19 ± 0.01 *(6)*	2063	1.62 ± 0.34 *(3)*	888
	7.4	0.44 ± 0.10 *(6)*	891	1.27 ± 0.24 *(3)*	1133
3-PNaA	6.0	0.33 ± 0.07 *(7)*	1188	1.04 ± 0.02 *(3)*	1384
	6.5	0.48 ± 0.11 *(7)*	817	1.53 ± 0.23 *(3)*	941
	7.0	0.39 ± 0.09 *(7)*	1005	1.35 ± 0.14 *(3)*	1066
	7.4	0.39 ± 0.10 *(7)*	1005	1.37 ± 0.12 *(3)*	1050
H-PNaA	6.0	0.44 ± 0.09 *(7)*	891	1.52 ± 0.26 *(3)*	947
	6.5	0.47 ± 0.11 *(7)*	834	1.79 ± 0.18 *(3)*	804
	7.0	0.46 ± 0.08 *(7)*	852	1.88 ± 0.11 *(3)*	765
	7.4	0.55 ± 0.06 *(7)*	713	1.58 ± 0.08 *(3)*	911

The three PNaA topologies were loaded with cisplatin and added to culture media at the specific pH values indicated. The pH values in culture medium (bicarbonate-free) were maintained with a phosphate buffer system. Exposure to PNaA-Pt (or free cisplatin as a control) was for 1 h and then permitted to recover for 24 h prior to the MTT assay on cell viability. The IC_{50} value to produce cytotoxicity was determined by regression of the general dose-response relationship. The Fold-Increase parameter refers to the improvement in potency (IC_{50}) afforded by the PNaA-Pt topologies compared to free cisplatin. All values refer to the mean ± SEM obtained from the number of independent observations indicated by the parentheses.

cisplatin-loaded polymer.

4. Discussion

Based on our *in vitro* observations, PNaA displays a number of features that render it a drug delivery system worthy of further development. All three polymer topologies are non-toxic to cells at concentrations likely to be adopted *in vivo*. Alkaline conditions enabled extensive loading of PNaA with cisplatin. Branched forms of the polymer displayed higher loading capacity, although structural features of branched polymers influenced the relationship between the extent of branching and loading. Unexpectedly, the anticipated release in an acidic environment was not realised and suggests that our initial hypothesis of a pH-dependent mechanism was overly simplistic. However, PNaA markedly increased the potency and efficacy of cisplatin to inhibit proliferation of cultured cancer cells, including those with resistance to the drug. This property and the versatile chemistry validate the potential of PNaA as a drug delivery system. The slow rate of interstitial cargo release supported a mechanism that involves internalisation of the drug-polymer complex. Although this is a departure from our original hypothesis, the property suggests the possibility of negligible cargo leakage *in vivo*, a clear advantage for prospective drug delivery systems.

Toxicity and pharmacokinetic profiles are critical determinants for the success or failure of putative new drugs or drug delivery systems. Our initial *in vitro* characterisation of PNaA as a drug delivery system provides important toxicity information at the cellular level. Cargo bound to the polymer should produce the anticancer activity through apoptosis, and not through a general necrotic pathway [41] caused by native PNaA *per se*. The latter effect would have adverse implications to non-cancerous tissue *in vivo* or in patients. Observations with native PNaA indicate that the polymer does not produce cell cycle arrest or any significant apoptotic or necrotic response in cultured cancer cells. This contrasts with the cell cycle arrest produced by structurally similar drug delivery systems including the natural poly(γ-glutamic acid) and the synthetic poly(methyl methacrylate) and poly(vinyl chloride) systems [42–44]. The absence of cell cycle arrest by PNaA ensures continued vulnerability of the target cancer cells to chemotherapeutic agents including cisplatin that target specific stages of the cycle [41]. Although native PNaA could produce cytotoxicity of cultured cancer cells, the IC_{50} values were clearly high and beyond levels likely to be required *in vivo* to deliver sufficient amounts of cisplatin. In addition, the native polymer only elicited apoptosis at the highest administered concentrations and for extended incubation periods. Similar profiles for the inherent toxicity of native polymers have been observed in a number of drug delivery systems [45–47].

Multiple investigations have outlined the potential or feasibility of polymer systems to enhance delivery of platinum to cancer cells [48,49]. A specific and significant advantage of PNaA as a delivery system for cisplatin (and derivatives) is the ease of cargo attachment via a ligand exchange reaction that requires no alteration of polymer composition. Loading capacity was assessed using ICP-MS to reveal the amount of platinum and also by CE. The latter assesses changes in polymer mobility due to charge alteration following loading and modulated hydrodynamic friction, which measures topology and heterogeneity [26,50]. The two branched PNaA topologies were developed to increase loading capacity compared to the linear form and potentially to generate multi-phase cargo release. Our observations demonstrated higher platinum loading in the two branched PNaA topologies, although the linear form has a lower pK_a [51]and thus more available carboxylate moieties than the branched ones. This may indicate incomplete digestion or the incomplete molecular solubility (solvation) of branched PNaAs [52]. In addition, the hyperbranched PNaA displayed similar platinum loading and mobility perturbations to the 3-arm star topology, despite their differences in branching and structural complexity. Overall, the more complex, branched PNaA configurations did not exhibit increases in loading capacity proportional to their theoretical number of cargo-binding sites. This may reflect impaired access to core regions of the polymer once surface sites become occupied. Alternatively, cargo-induced conformational changes may restrict further penetration, or heterogeneity in the polymer microenvironment may generate variable local affinities and loading efficiencies. Investigations with dendrimers and polymer complexes also indicate that more branching

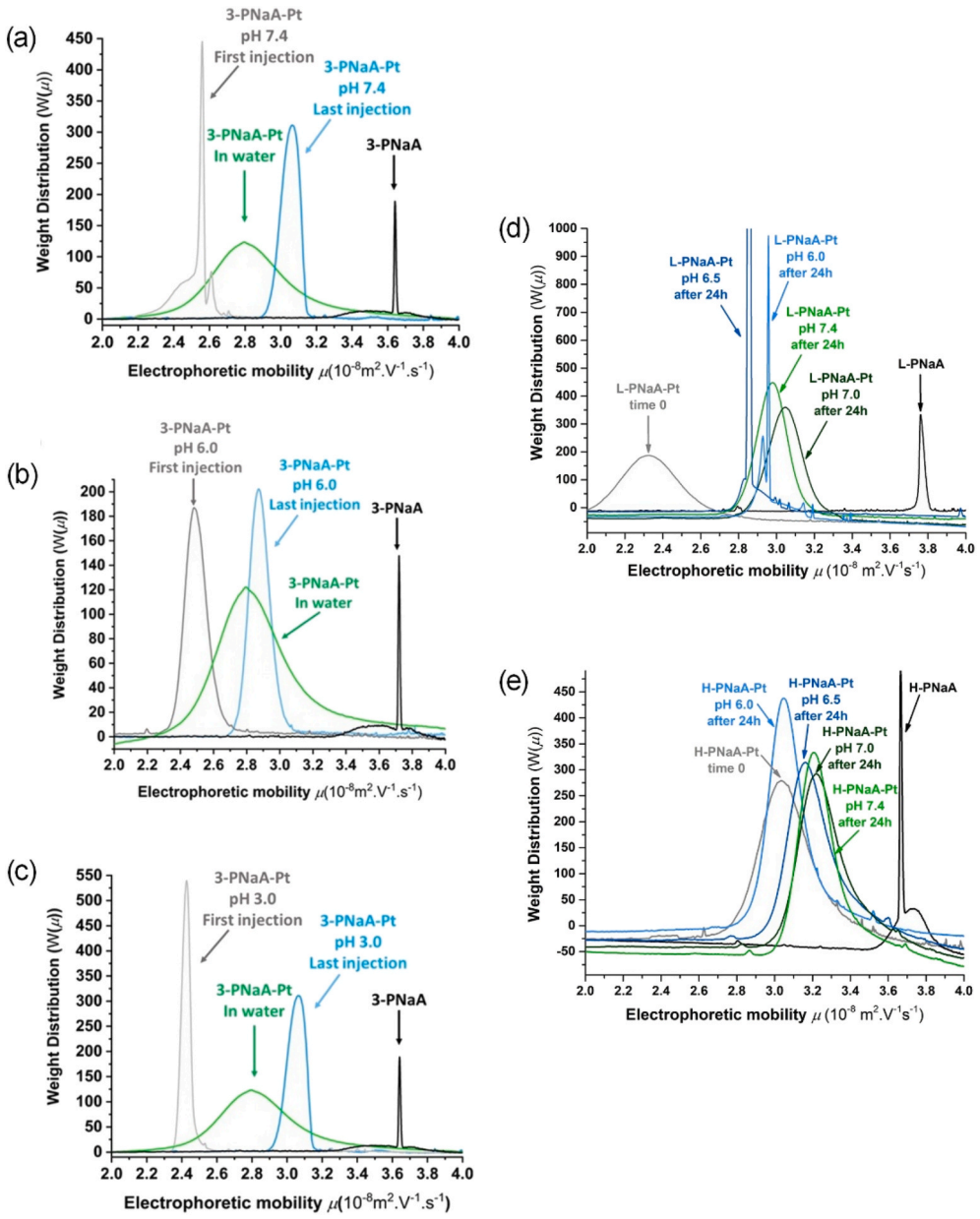

Fig. 7. Changes in distributions of electrophoretic mobilities of PNaA following platinum release.
The distributions of mobilities of PNaA were monitored using CE in a series of buffer conditions. Distributions of the empty PNaA are shown in *black* within each panel and the distribution of polymer loaded with cisplatin in water is shown in *green*. Polymer that had been loaded with cisplatin was added to solutions with specific pH values and a sample was immediately injected (*grey profile*). Samples were left in the different buffer conditions for up to 24 h and distributions of electrophoretic mobilities obtained periodically. The final samples injected (*blue and green profiles*) are shown within each panel and show the changes in Pt-PNaA mobility over the 24 h period. Panel assignments are as follows: (a) 3-PNaA-Pt at pH 7.4; (b) 3-PNaA-Pt at pH6.0; (c) 3-PNaA-Pt at pH3.0 and (d) L-PNaA-Pt at pHs 6.0, 6.5, 7.0 and 7.4; (e) H-PNaA at pHs 6.0, 6.5, 7.0 and 7.4. (For interpretation of the references to colour in this figure legend, the reader is referred to the Web version of this article.)

structures are associated with improved loading capacities, although the relationships are also not quantitatively related to the number of attachment sites [14,53,54]. We suggest that the excessive branching structure in PNaA shields many of the attachment structures within the core of its 3-D structure.

Our most important observation was that attachment of cisplatin to PNaA markedly improves the *in vitro* drug efficacy in multiple cell lines compared to drug *per se*. This warrants further development of the polymer as a drug delivery system. Capillary electrophoresis confirmed that PNaA releases its cargo in a pH-dependent manner. However, the enhanced cytotoxicity observed in cell-based assays did not display a corresponding pH dependence. This apparent discrepancy is likely due to the substantially slower rate of cargo release relative to the rapid kinetics of endocytic uptake. Other possible contributing factors include rapid rebinding of the released cisplatin to carboxylate groups within PNaA, an insufficient pH shift to trigger efficient cargo release, or structural features of the more complex PNaA conformations that impede hydration and release from deeper regions of the polymer. Previous investigations using PAA/PNaA as a component of drug delivery systems suggested that efficacy of the drug cargo was pH dependent. However, the PAA was not administered in isolation in these investigations. The PAA was incorporated into larger structures such as within the lumen of metallic microspheres [55], as a gel-composite [56] or in an end-capping function with hollow mesoporous carbon spheres

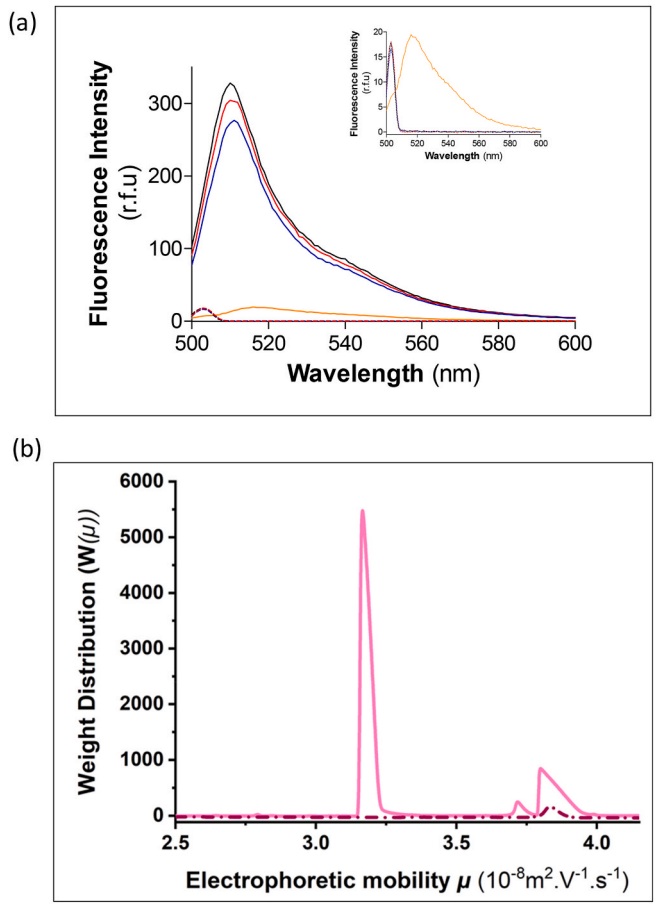

Fig. 8. Biophysical properties of BODIPY-labelled PnaA (a) Fluorescence emission spectra for PNaA with covalently attached BODIPY were obtained using an excitation wavelength of 488 nm (5 nm slit width). Spectra for BODIPY conjugated L-PNaA (*black*), 3-PNaA (*blue*) and H-PNaA (*red*) are shown as solid lines in the main figure. The emission spectrum for free BODIPY is shown in orange in the inset and the three versions of native (not loaded) PNaA are shown as dashed lines in the inset. (b) Distributions of electrophoretic mobilities are shown for native (*dashed line*) and BODIPY-attached versions (*solid line*) of L-PNaA. (For interpretation of the references to colour in this figure legend, the reader is referred to the Web version of this article.)

[57]. Consequently, a direct attribution of pH-dependency on the polymer might be considered tenuous. There are further alternative possible explanations for the lack of pH-dependency when using PNaA as an isolated polymer, based on its internal microenvironment. In its linear conformation, PNaA has a pK_a ~6.2, which rises to pK_a ~6.7 in the hyperbranched architecture [51] and these properties render it ideal for delivery to the tumour micro-environment, which is shown to display a pH range of 6.4-6.8 [58–60]. However, the binding or release of platinum containing groups may alter the local or global pK_a and thereby modulate the release range for PNaA. Alternatively, the kinetics of overall cargo release may be influenced by subsequent rebinding elsewhere on the polymer, which may be exacerbated with local fluctuations in environment or pK_a, particularly within the less accessible regions of branched PNaA topologies. Due to constraints with cultured cell viability, the pH-dependence data was restricted to the pH range 6-7.4, which is in the pathophysiological range.

As noted previously, the size of PNaA renders it amenable to internalisation via endocytic pathways. The high avidity of uptake may be driven by the elevated surface charge density of PNaA, which promotes favourable ionic interactions with the negatively charged cell surface. Additionally, PNaA may alter membrane dynamics in a manner that enhances internalisation. The rapid internalisation of polymeric structures has considerable precedent in the literature. For example, nano- and microplastic particles comprising poly(methyl methacrylate) or poly(vinyl chloride) enter BHK21 fibroblast cells via endocytosis, using a dynamin dependent route [43]. Unlike PNaA, these polymers displayed considerable inherent cytotoxicity, eliciting ROS generation and ATP depletion. In a manner similar to PNaA, their distribution was spread between the cytoplasm and inside perinuclear vesicular structures. Internalisation was also observed for poly(MePEGCA-co-HDCA) and like PNaA, it only affected cell viability with prolonged incubation at high concentrations and its distribution was primarily in lysosomes/endosomes in the perinuclear region [61]. The closely related poly(α-glutamic acid) copolymer displayed a similar pattern of distribution in the cell to PNaA and the authors observed intra-lysosomal release of doxorubicin cargo to achieve cell cytotoxicity [62]. It has been proposed that polymer internalisation through an endocytic uptake route is a general phenomenon, with cargo such as anthracyclines or platinating drugs liberated within the acidic luminal compartment [63]. We have demonstrated that PNaA is able to deliver high concentrations of cisplatin to cancer cells, but the mechanism leading to improved drug efficacy involves internalisation rather than the liberation of drug in the extracellular environment. Furthermore, the lack of cytotoxicity of PNaA *per se* suggests that the improved cytotoxicity of cisplatin may involve acid-dependent release of cargo. Since PNaA is internalised, a candidate route for cargo release may involve the endosomal-lysosomal compartment, although this has not been fully elucidated.

Drug delivery systems enhance the pharmacokinetic profiles of anticancer drugs by improving stability, enhancing serum half-life and delivering high concentrations to the site of action. However, an unforeseen benefit appears to be the ability to overcome resistance mechanisms [64–66]. Resistance conferred by multidrug efflux pumps is particularly amenable to circumvention by delivery systems. The efflux pumps are located at the plasma membrane and expel drugs prior to their passage into the cytoplasm; consequently, the endocytic uptake of polymers and nanoparticles will bypass the influence of these pumps. Resistance to cisplatin is multifactorial, but the major factors are considered to be gene silencing via methylation of the DNA-repair protein MLH1 [67,68] and/or the actions of ATP Binding Cassette (ABC) transporters to effect extrusion [69]. This former is corroborated by the ability of the DNA methylation inhibitor, Azadeoxycytidine, to restore the sensitivity of resistant A2780cis cells to cisplatin [70]. Based on these mechanisms, how can macromolecular drug delivery systems overcome cisplatin resistance? It has been demonstrated that liposomal, albumin and polymer-based delivery systems for cisplatin are all capable of circumventing the resistant phenotype in A2780cis cancer cells [71,72]. It is thought that the drug efflux activity of ABC transporters can be overwhelmed by the ability of delivery systems to produce such a direct and marked increase in cytoplasmic levels of cisplatin [7]. Our observations of rapid and extensive internalisation of PNaA-Pt coupled with the concomitant, major increase in cytotoxic efficacy implies a similar underlying mechanism. This internalisation mechanism has been confirmed in multiple studies using both cancer cells and at sites of physiological ABC transporter expression [73–75]. In all cases, the mechanism involves the direct delivery of drugs to the cytoplasm by the polymer (i.e. via internalisation) and avoiding the transmembrane diffusion of drug. The latter process is vulnerable to outward efflux of drugs by multidrug transporters.

5. Conclusion

Despite the availability of numerous drug delivery systems, their benefit has yet to translate significantly into clinical use. However, new systems and molecules have emerged from the extensive body of fundamental research. PNaA is one such macromolecule and this investigation suggests it is worthy of further assessment as a drug delivery system. PNaA has minimal inherent effects on cell viability or growth, rendering its toxicity profile favourable compared to other

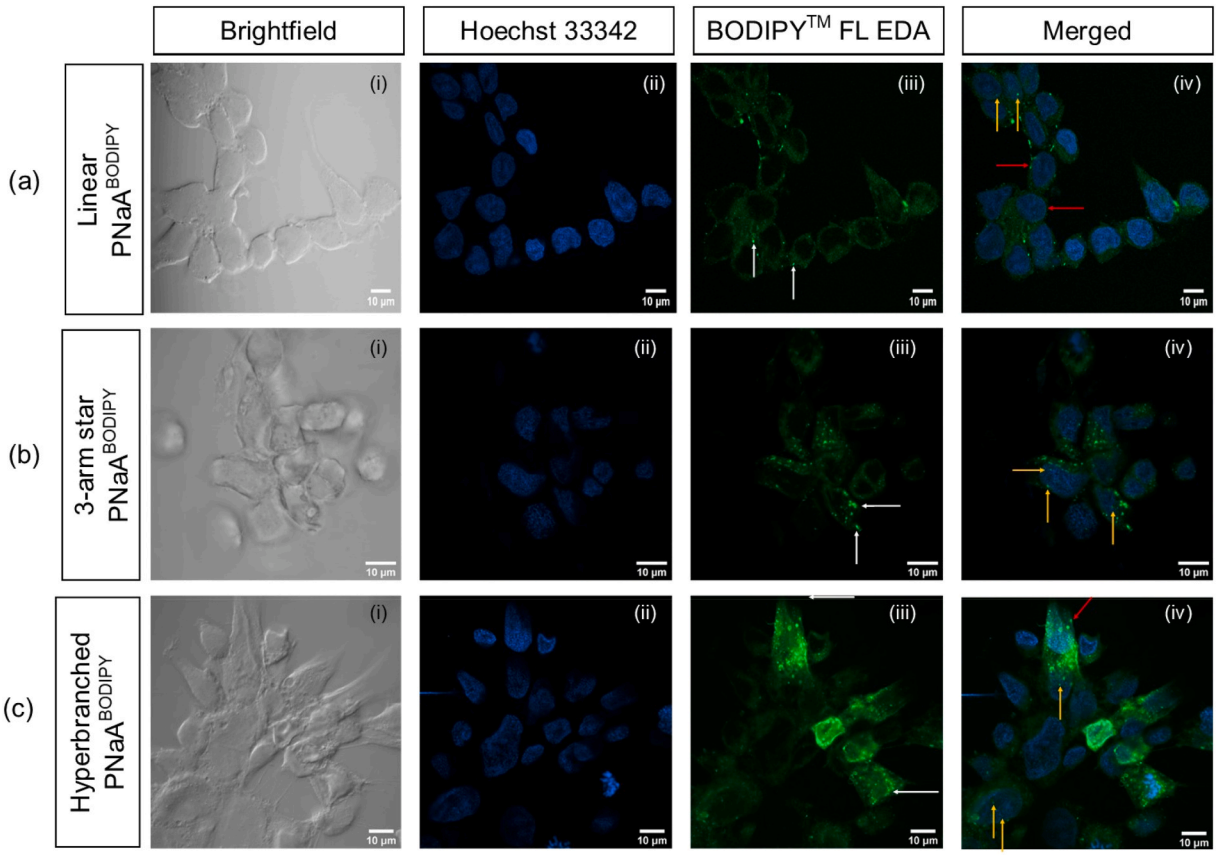

Fig. 9. Uptake and localisation of ^{BODIPY}PNaA in DLD1 cells.
Brightfield (*panels marked (i)*) and fluorescent micrographs of DLD1 cells exposed to the three topologies of PNaA (*panels marked (iii)*) with covalently attached BODIPY (*green stain*). The cells were counter-stained with Hoechst33342 (*blue stain*) to define the cell nuclei (*panels marked (ii)*). The panels on the right-hand side (*marked (iv)*) correspond to merged images of the BODIPY and Hoechst33342 channels. Arrows in the panels indicate the location of bright punctate spots (*white*), the perinuclear region (*red*) and possible nuclear localised polymer (*orange*). Cells were exposed to polymer (1000 μg/ml) for 15 min and to Hoechst33342 for 10 min prior to microscopy imaging. (For interpretation of the references to colour in this figure legend, the reader is referred to the Web version of this article.)

polymers. The polymer has simple and versatile chemistry that enables stable and reversible cargo attachment. Furthermore, PNaA may be readily conjugated with groups to facilitate polymer imaging *in vivo* or specific targeting to tumour markers. PNaA is rapidly internalised by cancer cells, giving rise to markedly improved cytotoxicity for the cisplatin cargo and the high capacity delivery to the cell interior may overcome the resistant phenotype. These advantageous properties of PNaA warrant further investigation as a drug delivery system. In particular, the use of *in vivo* models is the logical next step to provide rigorous measurement of whole-body toxicity and clearance in addition to assessment of targeting systems.

CRediT authorship contribution statement

E.G. Whitty: Conceptualization, Formal analysis, Investigation, Methodology, Writing – review & editing. **I. Sousa:** Investigation, Methodology, Writing – review & editing. **M. Gaborieau:** Conceptualization, Formal analysis, Funding acquisition, Supervision, Writing – review & editing. **P. Castignolles:** Conceptualization, Formal analysis, Funding acquisition, Supervision, Writing – review & editing. **R. Callaghan:** Conceptualization, Formal analysis, Funding acquisition, Project administration, Supervision, Writing – original draft.

Declaration of competing interest

The authors declare that they have no known competing financial interests or personal relationships that could have appeared to influence the work reported in this paper.

Acknowledgements

The authors thank the Australian National University and the Research School of Biology for providing a PhD scholarship to E Whitty and block grant funding for the project. MG and PC thank Dr Catherine Lefay and Dr Yohann Guillaneuf (Aix-Marseille University) for providing some of the polymers, SEC data and for invaluable discussions from the beginning of the project, as well as Alison Maniego for performing the FTIR measurements, assistance with performing capillary electrophoresis experiments and discussions about cisplatin loading to and release from PNaA. We would like to thank the assistance of Prof Trevor Hambley and Elisabeth Tondl at the University of Sydney, School of Chemistry for their invaluable assistance with the ICP-MS procedure.

Appendix A. Supplementary data

Supplementary data to this article can be found online at https://doi.org/10.1016/j.jddst.2026.108326.

Data availability

Data will be made available on request.

References

[1] M.S. Galanski, M.A. Jakupec, B.K. Keppler, Update of the preclinical situation of anticancer platinum complexes: novel design strategies and innovative analytical approaches, Curr. Med. Chem. 12 (18) (2005) 2075–2094.
[2] P.A. Andrews, S.B. Howell, Cellular pharmacology of cisplatin: perspectives on mechanisms of acquired resistance, Cancer Cells (Cold Spring Harbor) 2 (2) (1990) 35–43.
[3] M.D. Hall, H.R. Mellor, R. Callaghan, T.W. Hambley, Basis for design and development of platinum(IV) anticancer complexes, J. Med. Chem. 50 (15) (2007) 3403–3411.
[4] D. Wang, S.J. Lippard, Cellular processing of platinum anticancer drugs, Nat. Rev. Drug Discov. 4 (4) (2005) 307–320.
[5] H. An, C. Yang, Z. Jiang, J. Yuan, Z. Qiu, L. Chen, X. Chen, M. Huang, L. Huang, H. Lin, B. Cheng, H. Liu, Z. Yu, Luminescence-activated Pt(IV) prodrug for in situ triggerable cancer therapy, Chin. Chem. Lett. 35 (7) (2024) 109134.
[6] H. Fu, P. Liang, Q. Chen, Y. Wang, G. Li, X. Cai, S. Wang, K. Chen, S. Shi, Z. Yu, X. Wang, COX-2 blocking therapy in cisplatin chemosensitization of ovarian cancer: an allicin-based nanomedicine approach, Chin. Chem. Lett. 35 (8) (2024) 109241.
[7] H.R. Mellor, R. Callaghan, Resistance to chemotherapy in cancer: a complex and integrated cellular response, Pharmacology 81 (4) (2008) 275–300.
[8] P. Sapra, T.M. Allen, Ligand-targeted liposomal anticancer drugs, Prog. Lipid Res. 42 (5) (2003) 439–462.
[9] S. Dilruba, G.V. Kalayda, Platinum-based drugs: past, present and future, Cancer Chemother. Pharmacol. 77 (6) (2016) 1103–1124.
[10] T.M. Allen, P.R. Cullis, Liposomal drug delivery systems: from concept to clinical applications, Adv. Drug Deliv. Rev. 65 (1) (2013) 36–48.
[11] E. Beltrán-Gracia, A. López-Camacho, I. Higuera-Ciapara, J.B. Velázquez-Fernández, A.A. Vallejo-Cardona, Nanomedicine review: clinical developments in liposomal applications, Cancer Nanotechnology 10 (1) (2019) 11.
[12] F.U. Din, W. Aman, I. Ullah, O.S. Qureshi, O. Mustapha, S. Shafique, A. Zeb, Effective use of nanocarriers as drug delivery systems for the treatment of selected tumors, Int. J. Nanomed. 12 (2017) 7291–7309.
[13] W. Zhang, Z. Zhang, Y. Zhang, The application of carbon nanotubes in target drug delivery systems for cancer therapies, Nanoscale Res. Lett. 6 (1) (2011) 555.
[14] M. Callari, J.R. Aldrich-Wright, P.L. de Souza, M.H. Stenzel, Polymers with platinum drugs and other macromolecular metal complexes for cancer treatment, Prog. Polym. Sci. 39 (9) (2014) 1614–1643.
[15] Y. Mochida, H. Cabral, K. Kataoka, Polymeric micelles for targeted tumor therapy of platinum anticancer drugs, Expet Opin. Drug Deliv. 14 (12) (2017) 1423–1438.
[16] N. Deirram, C. Zhang, S.S. Kermaniyan, A.P.R. Johnston, G.K. Such, pH-Responsive polymer nanoparticles for drug delivery, Macromol. Rapid Commun. 40 (10) (2019) e1800917.
[17] C.M. Wells, M. Harris, L. Choi, V.P. Murali, F.D. Guerra, J.A. Jennings, Stimuli-responsive drug release from smart polymers, J. Funct. Biomater. 10 (3) (2019) 34.
[18] E.G. Whitty, A.R. Maniego, S.A. Bentwitch, Y. Guillaneuf, M.R. Jones, M. Gaborieau, P. Castignolles, Cellular response to linear and branched poly (acrylic acid), Macromol. Biosci. 15 (12) (2015) 1724–1734.
[19] A.R. Maniego, D. Ang, Y. Guillaneuf, C. Lefay, D. Gigmes, J.R. Aldrich-Wright, M. Gaborieau, P. Castignolles, Separation of poly(acrylic acid) salts according to topology using capillary electrophoresis in the critical conditions, Anal. Bioanal. Chem. 405 (28) (2013) 9009–9020.
[20] O.E. Philippova, D. Hourdet, R. Audebert, A.R. Khokhlov, pH-Responsive gels of hydrophobically modified poly(acrylic acid), Macromolecules 30 (26) (1997) 8278–8285.
[21] E. Cabane, X. Zhang, K. Langowska, C.G. Palivan, W. Meier, Stimuli-responsive polymers and their applications in nanomedicine, Biointerphases 7 (1–4) (2012) 9.
[22] A. Kumar, A. Srivastava, I.Y. Galaev, B. Mattiasson, Smart polymers: physical forms and bioengineering applications, Prog. Polym. Sci. 32 (10) (2007) 1205–1237.
[23] M. Simeonov, A. Monova, B. Kostova, E. Vassileva, Drug transport in stimuli responsive acrylic and methacrylic interpenetrating polymer networks, J. Appl. Polym. Sci. 134 (42) (2017) 45380.
[24] A.R. Maniego, A.T. Sutton, Y. Guillaneuf, C. Lefay, M. Destarac, C.M. Fellows, P. Castignolles, M. Gaborieau, Degree of branching in poly(acrylic acid) prepared by controlled and conventional radical polymerization, Polym. Chem. 10 (19) (2019) 2469–2476.
[25] I. Lacík, M. Stach, P. Kasák, V. Semak, L. Uhelská, A. Chovancová, G. Reinhold, P. Kilz, G. Delaittre, B. Charleux, I. Chaduc, F. D'Agosto, M. Lansalot, M. Gaborieau, P. Castignolles, R.G. Gilbert, Z. Szablan, C. Barner-Kowollik, P. Hesse, M. Buback, SEC analysis of Poly(Acrylic acid) and Poly(Methacrylic acid), Macromol. Chem. Phys. 216 (1) (2015) 23–37.
[26] J.J. Thevarajah, A.T. Sutton, A.R. Maniego, E.G. Whitty, S. Harrisson, H. Cottet, P. Castignolles, M. Gaborieau, Quantifying the heterogeneity of chemical structures in complex charged polymers through the dispersity of their distributions of electrophoretic mobilities or of compositions, Anal. Chem. 88 (3) (2016) 1674–1681.
[27] D. Muthiah, R. Callaghan, Dual effects of the PI3K inhibitor ZSTK474 on multidrug efflux pumps in resistant cancer cells, Eur. J. Pharmacol. 815 (2017) 127–137.
[28] H.R. Mellor, S. Snelling, M.D. Hall, S. Modok, M. Jaffar, T.W. Hambley, R. Callaghan, The influence of tumour microenvironmental factors on the efficacy of cisplatin and novel platinum(IV) complexes, Biochem. Pharmacol. 70 (8) (2005) 1137–1146.
[29] O. Hayes, B. Ramos, L.L. Rodríguez, A. Aguilar, T. Badía, F.O. Castro, Cell confluency is as efficient as serum starvation for inducing arrest in the G0/G1 phase of the cell cycle in granulosa and fibroblast cells of cattle, Anim. Reprod. Sci. 87 (3–4) (2005) 181–192.
[30] E. Wintersberger, I. Mudrak, Sodium butyrate inhibits the synthesis of the transformation related protein p 53 in 3T6 mouse fibroblasts, FEBS Lett. 166 (2) (1984) 326–330.
[31] F.D. Ragione, V. Cucciolla, A. Borriello, V.D. Pietra, L. Racioppi, G. Soldati, C. Manna, P. Galletti, V. Zappia, Resveratrol arrests the cell division cycle at S/G2 phase transition, Biochem. Biophys. Res. Commun. 250 (1) (1998) 53–58.
[32] R. Kuriyama, Effect of colcemid on the centriole cycle in Chinese hamster ovary cells, J. Cell Sci. 53 (1982) 155–171.
[33] J. Muppidi, M. Porter, R.M. Siegel, Measurement of apoptosis and other forms of cell death, Current protocols in immunology Chapter 3 (2004). Unit 3.17.
[34] P. Castignolles, M. Gaborieau, E.F. Hilder, E. Sprong, C.J. Ferguson, R.G. Gilbert, High-resolution separation of Oligo(acrylic acid) by capillary zone, Electrophoresis 27 (1) (2006) 42–46.
[35] A. Sutton, N. University of South Australia, E. School of, I. Built, University of South Australia. Future Industries, Improving the Sustainability of Analytical Separation Science, 2019. Thesis (PhD(Environmental Science and Engineering))–University of South Australia, 2019.
[36] K.R. Riley, S. Liu, G. Yu, K. Libby, R. Cubicciotti, C.L. Colyer, Using capillary electrophoresis to characterize polymeric particles, J. Chromatogr. A 1463 (2016) 169–175.
[37] G. Hermann, P. Heffeter, T. Falta, W. Berger, S. Hann, G. Koellensperger, In vitro studies on cisplatin focusing on kinetic aspects of intracellular chemistry by LC-ICP-MS, Metallomics 5 (6) (2013) 636–647.
[38] A.R. Timerbaev, S.S. Aleksenko, K. Polec-Pawlak, R. Ruzik, O. Semenova, C. G. Hartinger, S. Oszwaldowski, M. Galanski, M. Jarosz, B.K. Keppler, Platinum metallodrug-protein binding studies by capillary electrophoresis-inductively coupled plasma-mass spectrometry: characterization of interactions between Pt(II) complexes and human serum albumin, Electrophoresis 25 (13) (2004) 1988–1995.
[39] L. Kou, J. Sun, Y. Zhai, Z. He, The endocytosis and intracellular fate of nanomedicines: implication for rational design, Asian J. Pharm. Sci. 8 (1) (2013) 1–10.
[40] S. Zhang, J. Li, G. Lykotrafitis, G. Bao, S. Suresh, Size-dependent endocytosis of nanoparticles, Adv. Mater. 21 (2009) 419–424.
[41] A.H. Abouzeid, V.P. Torchilin, The role of cell cycle in the efficiency and activity of cancer nanomedicines, Expet Opin. Drug Deliv. 10 (6) (2013) 775–786.
[42] B. Liu, C. Che, J. Liu, M. Si, Z. Gong, Y. Li, J. Zhang, G. Yang, Fabrication and antitumor mechanism of a nanoparticle drug delivery system: Graphene oxide/chitosan Oligosaccharide/γ-Polyglutamic acid composites for anticancer drug delivery 4 (43) (2019) 12491–12502.
[43] G. Mahadevan, S. Valiyaveettil, Understanding the interactions of poly(methyl methacrylate) and poly(vinyl chloride) nanoparticles with BHK-21 cell line, Sci. Rep. 11 (1) (2021) 2089.
[44] N. Qi, B. Tang, G. Liu, X. Liang, Poly(γ-glutamic acid)-coated lipoplexes loaded with doxorubicin for enhancing the antitumor activity against liver tumors, Nanoscale Res. Lett. 12 (1) (2017) 361.
[45] W.H. De Jong, P.J.A. Borm, Drug delivery and nanoparticles: applications and hazards, Int. J. Nanomed. 3 (2) (2008) 133–149.
[46] A.U. Kura, S. Fakurazi, M.Z. Hussein, P. Arulselvan, Nanotechnology in drug delivery: the need for more cell culture based studies in screening, Chem. Cent. J. 8 (1) (2014) 46.
[47] W. Lin, Y.W. Huang, X.D. Zhou, Y. Ma, In vitro toxicity of silica nanoparticles in human lung cancer cells, Toxicol. Appl. Pharmacol. 217 (3) (2006) 252–259.
[48] E. Entezar-Almahdi, R. Heidari, S. Ghasemi, S. Mohammadi-Samani, F. Farjadian, Integrin receptor mediated pH-responsive nano-hydrogel based on histidine-modified poly(aminoethyl methacrylamide) as targeted cisplatin delivery system, J. Drug Deliv. Sci. Technol. 62 (2021) 102402.
[49] S. Ghasemi, M. Owrang, F. Javaheri, F. Farjadian, Spermine modified PNIPAAm nano-hydrogel serving as thermo-responsive system for delivery of cisplatin, Macromol. Res. 30 (5) (2022) 314–324.
[50] F. Oukacine, S. Bernard, I. Bobe, H. Cottet, Physico-chemical characterization of polymeric micelles loaded with platinum derivatives by capillary electrophoresis and related methods, J. Contr. Release 196 (2014) 139–145.
[51] F.A. Plamper, H. Becker, M. Lanzendörfer, M. Patel, A. Wittemann, M. Ballauff, A. H.E. Müller, Synthesis, characterization and behavior in aqueous solution of star-shaped poly(acrylic acid), Macromol. Chem. Phys. 206 (18) (2005) 1813–1825.
[52] A.R. Maniego, A.T. Sutton, M. Gaborieau, P. Castignolles, Assessment of the branching quantification in poly(acrylic acid): is it as easy as it seems? Macromolecules 50 (22) (2017) 9032–9041.
[53] J.J. Khandare, S. Jayant, A. Singh, P. Chandna, Y. Wang, N. Vorsa, T. Minko, Dendrimer versus linear conjugate: influence of polymeric architecture on the delivery and anticancer effect of paclitaxel, Bioconjug. Chem. 17 (6) (2006) 1464–1472.
[54] L.Y. Qiu, Y.H. Bae, Polymer architecture and drug delivery, Pharm. Res. 23 (1) (2006) 1–30.
[55] Y. Dai, C. Zhang, Z. Cheng, P. Ma, C. Li, X. Kang, D. Yang, J. Lin, pH-responsive drug delivery system based on luminescent CaF(2):Ce(3+)/Tb(3+)-poly(acrylic acid) hybrid microspheres, Biomaterials 33 (8) (2012) 2583–2592.
[56] D. Ding, J. Wang, Z. Zhu, R. Li, W. Wu, B. Liu, X. Jiang, Tumor accumulation, penetration, and antitumor response of cisplatin-loaded gelatin/poly(acrylic acid) nanoparticles, ACS Appl. Mater. Interfaces 4 (3) (2012) 1838–1846.
[57] X. Li, C. Liu, S. Wang, J. Jiao, D. Di, T. Jiang, Q. Zhao, S. Wang, Poly(acrylic acid) conjugated hollow mesoporous carbon as a dual-stimuli triggered drug delivery system for chemo-photothermal synergistic therapy, Mater. Sci. Eng., C 71 (2017) 594–603.

[58] A. Silberman, O. Goldman, O. Boukobza Assayag, A. Jacob, S. Rabinovich, L. Adler, J.S. Lee, R. Keshet, A. Sarver, J. Frug, N. Stettner, S. Galai, E. Persi, K.B. Halpern, Y. Zaltsman-Amir, B. Pode-Shakked, R. Eilam, Y. Anikster, S.C.S. Nagamani, I. Ulitsky, E. Ruppin, A. Erez, Acid-induced downregulation of ASS1 contributes to the maintenance of intracellular pH in cancer, Cancer Res. 79 (3) (2019) 518–533.
[59] I.F. Tannock, D. Rotin, Acid pH in tumors and its potential for therapeutic exploitation, Cancer Res. 49 (16) (1989) 4373–4384.
[60] L. Zhu, P.P. Smith, S.G. Boyes, pH-responsive polymers for imaging acidic biological environments in tumors 51 (14) (2013) 1062–1067.
[61] M. Costanzo, F. Carton, A. Marengo, G. Berlier, B. Stella, S. Arpicco, M. Malatesta, Fluorescence and electron microscopy to visualize the intracellular fate of nanoparticles for drug delivery, Eur. J. Histochem. : EJH 60 (2) (2016) 2640.
[62] H. Xu, C. Cai, J. Gou, B. Sui, J. Jin, H. Xu, Y. Zhang, L. Wang, Y. Zhai, X. Tang, Self-assembled monomethoxy (polyethylene Glycol)-b-P(D,L-Lactic-co-Glycolic Acid)-b-P(L-Glutamic acid) hybrid-core nanoparticles for intracellular pH-Triggered release of doxorubicin, J. Biomed. Nanotechnol. 11 (8) (2015) 1354–1369.
[63] R. Duncan, Designing polymer conjugates as lysosomotropic nanomedicines, Biochem. Soc. Trans. 35 (Pt 1) (2007) 56–60.
[64] K. Cho, X. Wang, S. Nie, Z.G. Chen, D.M. Shin, Therapeutic nanoparticles for drug delivery in cancer, Clin. Cancer Res. : an official journal of the American Association for Cancer Research 14 (5) (2008) 1310–1316.
[65] W. Li, H. Zhang, Y.G. Assaraf, K. Zhao, X. Xu, J. Xie, D.H. Yang, Z.S. Chen, Overcoming ABC transporter-mediated multidrug resistance: molecular mechanisms and novel therapeutic drug strategies, Drug Resist. Updates : reviews and commentaries in antimicrobial and anticancer chemotherapy 27 (2016) 14–29.
[66] Q. Wang, H. Li, T. Wu, B. Yu, H. Cong, Y. Shen, Nanodrugs based on co-delivery strategies to combat cisplatin resistance, J. Contr. Release 370 (2024) 14–42.
[67] A. Sawant, A. Kothandapani, A. Zhitkovich, R.W. Sobol, S.M. Patrick, Role of mismatch repair proteins in the processing of cisplatin interstrand cross-links, DNA Repair 35 (2015) 126–136.
[68] C. Zeller, W. Dai, N.L. Steele, A. Siddiq, A.J. Walley, C.S. Wilhelm-Benartzi, S. Rizzo, A. van der Zee, J.A. Plumb, R. Brown, Candidate DNA methylation drivers of acquired cisplatin resistance in ovarian cancer identified by methylome and expression profiling, Oncogene 31 (42) (2012) 4567–4576.
[69] R.J. Parker, A. Eastman, F. Bostick-Bruton, E. Reed, Acquired cisplatin resistance in human ovarian cancer cells is associated with enhanced repair of cisplatin-DNA lesions and reduced drug accumulation, J. Clin. Investig. 87 (3) (1991) 772–777.
[70] P. Branch, M. Masson, G. Aquilina, M. Bignami, P. Karran, Spontaneous development of drug resistance: mismatch repair and p53 defects in resistance to cisplatin in human tumor cells, Oncogene 19 (28) (2000) 3138–3145.
[71] D. Garmann, A. Warnecke, G.V. Kalayda, F. Kratz, U. Jaehde, Cellular accumulation and cytotoxicity of macromolecular platinum complexes in cisplatin-resistant tumor cells, J. Contr. Release : official journal of the Controlled Release Society 131 (2) (2008) 100–106.
[72] M.L. Krieger, N. Eckstein, V. Schneider, M. Koch, H.D. Royer, U. Jaehde, G. Bendas, Overcoming cisplatin resistance of ovarian cancer cells by targeted liposomes in vitro, Int. J. Pharm. 389 (1–2) (2010) 10–17.
[73] K. AboulFotouh, A.A. Allam, M. El-Badry, A.M. El-Sayed, Self-emulsifying drug–delivery systems modulate P-Glycoprotein activity: role of excipients and formulation aspects, Nanomedicine 13 (14) (2018) 1813–1834.
[74] D. Goren, A.T. Horowitz, D. Tzemach, M. Tarshish, S. Zalipsky, A. Gabizon, Nuclear delivery of doxorubicin via folate-targeted liposomes with bypass of multidrug-resistance efflux pump, Clin. Cancer Res. 6 (5) (2000) 1949–1957.
[75] T.-T.-L. Nguyen, V.-A. Duong, H.-J. Maeng, Pharmaceutical formulations with P-Glycoprotein inhibitory effect as promising approaches for enhancing oral drug absorption and bioavailability, Pharmaceutics 13 (7) (2021) 1103.